1-1-2016

Assessing the effect of sequential extraction on the uranium-series isotopic composition of a basaltic weathering profile

Davide Menozzi
University of Wollongong, dm791@uowmail.edu.au

Anthony Dosseto
University of Wollongong, tonyd@uow.edu.au

Leslie Kinsley
Australian National University, leslie.kinsley@anu.edu.au

Assessing the effect of sequential extraction on the uranium-series isotopic composition of a basaltic weathering profile

Abstract

Soil sustainability implies maintaining the balance between soil erosion and production. While it is known how to assess soil erosion, only recently we have been able to estimate rates of soil and saprolite (namely regolith) production using uranium-series isotopes. This method assesses the time elapsed since rock-forming minerals start fractionating the U-series isotopes. In this study, we assess a sample pre-treatment protocol that has the potential to improve the method used to estimate regolith production rates. We propose that removal (or partial removal) of secondary phases precipitated from solution during pedogenesis (solution-derived phases) and organic matter from regolith may improve the accuracy of this method. This is tested using sequential extraction followed by etching as sample pre-treatment. Here, we assess their effect on the U-series isotopic composition of regolith and infer whether they minimize the presence of solution-derived phases and organic matter. We applied sequential extraction and etching to a basaltic weathering profile (bedrock, saprolite and soil) and compared the U-series isotopic composition before and after treatment. We also measured major elements concentrations and assessed mineralogy. The bedrock was in secular equilibrium and sequential extraction resulted in unchanged (234U/238U) activity ratios, while increased (230Th/238U). In contrast, etching resulted in increased (234U/238U) and (230Th/238U) activity ratios, which is attributed to the removal of primary minerals. Relative to the untreated bedrock, the untreated saprolite showed no changes in U and Th concentrations, and activity ratios. We hypothesise that during the conversion of bedrock into saprolite U and Th budgets are unaffected. Moreover, major element and mineralogical analyses suggest that during this process rock-forming minerals are converted into secondary phases (clays). We hypothesise that during this conversion the U-series isotopes are not fractionated; therefore, the removal of these secondary phases is not necessary. Relative to the saprolite, the soil showed gains of U and Th, (234U/238U) > 1 and (230Th/238U) < 1. This could result from precipitation of solution-derived phases from soil-pore water and/or nuclide adsorption onto organic matter. These phases were removed by sequential extraction, which resulted in a residue with (234U/238U) < 1 and (230Th/238U) > 1. To minimize the presence of solution-derived phases and organic matter in basaltic weathering profiles we suggest that only soil samples should undergo sequential extraction, because only these are significantly affected by solution-derived phases and organic matter. Additionally, our experiments show the existence of fractionation processes that are often overlooked in U-series isotopic studies, i.e. implantation of 234U and 230Th recoiled from U-rich mineral (i.e. glass) into adjacent, U-poor phases (e.g. pyroxene and feldspar).

Disciplines

Medicine and Health Sciences | Social and Behavioral Sciences

Publication Details

Menozzi, D., Dosseto, A. & Kinsley, L. P. J. (2016). Assessing the effect of sequential extraction on the uranium-series isotopic composition of a basaltic weathering profile. Chemical Geology, 446 126-137.

Assessing the effect of sequential extraction on the uranium-series isotopic composition of a basaltic weathering profile

Davide Menozzi[1,*], Anthony Dosseto[1] and Leslie P.J. Kinsley[2]

[1]*Wollongong Isotope Geochronology Laboratory, School of Earth & Environmental Sciences, University of Wollongong, Wollongong, NSW 2522, Australia.*
[2]*Research School of Earth Sciences, Australian National University, Canberra, ACT 0200, Australia.*

*Corresponding author: email: dm791@uowmail.edu.au
Telephone: (+61 2) 4221 3382

Abstract

Soil sustainability implies maintaining the balance between soil erosion and production. While it is known how to assess soil erosion, only recently we have been able to estimate rates of soil and saprolite (namely regolith) production using uranium-series isotopes. This method assesses the time elapsed since rock-forming minerals start fractionating the U-series isotopes. In this study, we assess a sample pre-treatment protocol that has the potential to improve the method used to estimate regolith production rates. We propose that removal (or partial removal) of secondary phases precipitated from solution during pedogenesis (*solution-derived phases*) and organic matter from regolith may improve the accuracy of this method. This is tested using sequential extraction followed by etching as sample pre-treatment. Here, we assess their effect on the U-series isotopic composition of regolith and infer whether they minimize the presence of solution-derived phases and organic matter.

We applied sequential extraction and etching to a basaltic weathering profile (bedrock, saprolite and soil) and compared the U-series isotopic composition before and after treatment. We also measured major elements concentrations and assessed mineralogy. The bedrock was in secular equilibrium and sequential extraction resulted in unchanged ($^{234}U/^{238}U$) activity ratios, while increased ($^{230}Th/^{238}U$). In contrast, etching resulted in increased ($^{234}U/^{238}U$) and ($^{230}Th/^{238}U$) activity ratios, which is attributed to the removal of primary minerals. Relative to the untreated bedrock, the untreated saprolite showed no changes in U and Th concentrations, and activity ratios. We hypothesise that during the conversion of bedrock into saprolite U and Th budgets are unaffected. Moreover, major elements and mineralogical analysis suggest that during this process rock-forming minerals are converted into secondary phases (clays). We hypothesis that during this conversion the U-series isotopes are not fractionated; therefore, the removal of these secondary phases is not necessary. Relative to the saprolite, the soil showed gains of U and Th, ($^{234}U/^{238}U$) >1 and ($^{230}Th/^{238}U$) <1. This could result from precipitation of solution-derived phases from soil-pore water and/or nuclide adsorption onto organic matter. These phases were removed by sequential extraction, which resulted in a residue with ($^{234}U/^{238}U$) <1 and ($^{230}Th/^{238}U$) >1. To minimize the presence of solution-derived phases and organic matter in basaltic weathering profiles we suggest that only soil samples should undergo sequential extraction, because only these are significantly affected by solution-derived phases and organic matter.

Finally, our experiments show the existence of fractionation processes that are often overlooked in U-series isotopic studies, i.e. implantation of ^{234}U and ^{230}Th recoiled from U-rich mineral (i.e. glass) into adjacent, U-poor phases (e.g. pyroxene and feldspar).

1. Introduction

Uranium-series isotopes can be used to estimate rates of regolith production and study weathering processes. This is because intermediate daughter nuclides of the U-series system have an array of half-lives that cover timescales of weathering processes (Chabaux et al., 2013; Chabaux et al., 2003; Dequincey et al., 2002; Dosseto et al., 2011; Dosseto et al., 2012; Dosseto et al., 2008; Ma et al., 2010; Suresh et al., 2013). For a system that has remained closed for more than 1 Myr, all U-series isotopes will be in secular equilibrium (i.e. daughter-parent activity ratios will be 1). When the bedrock starts weathering and its primary minerals dissolve, U-series isotopes fractionate and the solid residue deviates from secular equilibrium. The fractionation of the U-series isotopes reflects the nuclide chemical mobility, which is uranium-234 (^{234}U) >uranium-238 (^{238}U) >thorium-230 (^{230}Th) (Chabaux et al., 2003). As a result, weathering products, such as residual primary minerals found in regolith, are expected to show ($^{234}U/^{238}U$) <1 and ($^{230}Th/^{238}U$) >1, where parenthesis denote *activity ratios* through this article. In contrast, the solution that weathers primary minerals – such as soil-pore water – will be characterized by ($^{234}U/^{238}U$) >1 and ($^{230}Th/^{238}U$) <1 (Andersen et al., 2009; Chabaux et al., 2001). Hence, secondary phases precipitated from solution during pedogenesis (hereafter *solution-derived phases*) and organic matter, which is expected to adsorb U from solution, will show ($^{234}U/^{238}U$) >1 and ($^{230}Th/^{238}U$) <1 (Chabaux et al., 2003; Dequincey et al., 2002; Plater et al., 1992). Regolith is composed of *bedrock-derived phases* (i.e. residual primary minerals and secondary phases derived from their incongruent dissolution), solution-derived phases and organic matter.The U-series isotopic compositions of bulk regolith will represent the composition of all these components.

Regolith production rates can be estimated by modelling the evolution of U-series isotopic composition with profile depth. In a sample, the evolution of the abundance of a nuclide *j* (*Nj*) with time is described by the following equation (Dequincey et al., 2002; Dosseto et al., 2008c):

$$\frac{dN_j}{dt} = \lambda_i N_i - \lambda_j N_j + f_j N_{j,0} - k_j N_j$$

where t is time (yr), λ_i and λ_j are the decay constants (yr^{-1}) of the parent nuclide i and its daughter j, N_i is the number of the nuclide i in the sample, f_j is the *gain coefficient* of nuclide j (yr^{-1}) and k_j is the *loss coefficient* for j (yr^{-1}).

The model makes three main assumptions (Chabaux et al., 2013; Dosseto et al., 2012). Firstly, during regolith formation nuclides are continuously lost by dissolution of bedrock-derived phases. Secondly, nuclides are continuously gained due to precipitation of solution-derived phases, adsorption on organic matter and dust deposition. Note that the assumption of constant nuclides loss and gain implies that regolith production rates estimated by the model are values integrated over the time of regolith formation. Lastly, nuclide loss and gain occur over a similar timescale. Dosseto et al. (2012) pointed out that the third assumption is a potential drawback of the model, as nuclides gain and loss may operate at different timescales. In addition, several studies have shown that U-series isotope mobility may vary throughout a regolith (e.g. greater mobility of Th relative to U) particularly in upper horizons of weathering profiles (Dosseto et al., 2008b; Gontier et al., 2015; Ma et al., 2010; Rezzoug et al., 2009; Rihs et al., 2011). This can be due to external input of nuclides (e.g. precipitation of solution-derived phases) and/or processes involving organic matter in soil (e.g. organic matter may increase Th mobility; Chabaux et al., 2008; Chabaux et al., 2003). These considerations suggest that minimization of the contribution of solution-derived phases and organic matter to regolith isotopic composition could improve the model used to estimate regolith production rates. Removal of solution-derived phases and organic matter would limit the importance of the second and third assumptions. However, until now, regolith production rates have been estimated analysing untreated material (Chabaux et al., 2013; Dequincey et al., 2002; Dosseto et al., 2011; Dosseto et al., 2006; Dosseto et al., 2008b; Vigier et al., 2001).

A possible approach to remove solution-derived phases and organic matter is sequential chemical extraction. *Sequential extraction* has been designed to partition trace metals contained in soil into four, operationally-defined fractions: exchangeables, carbonates, Fe- and Mn-oxides and organic matter (Schultz et al., 1998; Tessier et al., 1979). In the case of U-series isotopes, few authors have studied the effect of this approach on soil (Blanco et al., 2004, 2005; Handley et al., 2013; Lee, 2009; Martin et al., 2015; Suresh et al., 2014; Suresh et al., 2013). Sequential extraction has been tested in the context of the comminution age theory, where it was applied to both marine and continental sediments (Lee, 2009; Martin et al., 2015). For instance, Martin et al. (2015) tested the effectiveness of sequential extraction in removing

secondary phases from a soil, marine and river sediments. They found that i) the removal of the secondary phases can be effectively monitored by measuring ($^{234}U/^{238}U$), ii) ($^{234}U/^{238}U$) decreases during sequential extraction as secondary phases are removed, and iii) additional mild HF/HCl etching further decreases ($^{234}U/^{238}U$) to a minimum, which indicates additional removal of secondary phases. Similar experiments were carried out by Suresh et al. (2014; 2013). However, these studies focused on top soil, and the rest of regolith was not considered (i.e. saprolite). Here, we test whether the approach proposed by Martin et al. (2015) can be extended to an entire regolith profile. We monitored the U-series isotopic composition and U and Th concentrations of bedrock, saprolite and soil samples before and after sequential extraction, and during a 24-hr mild HF/HCl etching. The primary target of this study is to test the effect of sequential extraction and etching on U-series isotopic composition of regolith. This information, combined with mineralogical and major element analyses, is used to assess whether this sample pre-treatment reduces the presence of solution-derived phases and organic matter in regolith.

2. Materials and methods

2.1 Environmental setting

The study area is located in Exeter, New South Wales, Australia (34°37'15.05" S 150° 19'08.30" E). The locality is at an elevation of 718 m and receives an annual average rainfall between 500 and 2000 mm. The underlying bedrock is a tertiary basalt and K-Ar dating measurements, carried on surrounding extrusions, have provided age estimates between 45 and 53 My (Wellman and McDougall, 1974). The soil is classified as Kraznozemic and consists of brown clays with high sesquioxide content and shows minor change in texture through the profile (Young, 1982). The Australian Soil Resource Information System classifies the land cover as grazing natural vegetation. Samples were collected from a ridge top area in order to minimize input of colluvium due to lateral transport. A 2.7 meter-deep core was collected using a mechanical drilling system until the underlying bedrock was reached. Two soils (S_{UP} and S_{LOW}), two saprolites (C_{UP} and C_{LOW}) and bedrock (BR) were collected respectively at 0.1, 0.9, 1.9, 2.5 and 2.7 m.

2.2 Analytical techniques

A thin section of the bedrock was prepared for optical analysis. The bedrock was ground, water washed using deionized water and dried in an oven at 60°C, before sequential extraction and etching. Soil and saprolite samples were dried in an oven at 60°C and an aliquot was analysed

as *untreated* sample for U-series, major elements and Loss on Ignition (LOI) analysis. A second aliquot was homogenized with an agate mortar and wet sieved; the size fraction between 125 and 2000 µm was retained and underwent sequential extraction and etching. The grain size fraction coarser than 125 µm was retained in order to minimize dust contribution, which could significantly affect the U-series isotopic composition of regolith (Pelt et al., 2013). A cut-off size of 125 µm was chosen because æolian material is composed of particles smaller than ~100 µm in the study area (Cattle et al., 2009). In order to assess the effect of sieving, major element and U-series isotopic analyses were performed before and after sieving. The samples were prepared at Wollongong Isotope Geochronology Laboratory, University of Wollongong.

For sequential extraction, about 2 g of sample were placed in 50 ml perfluoroalkoxy alkane (PFA) centrifuge tubes. Sequential extraction followed the procedure proposed by Tessier et al (1979), with one modification: the exchangeable fraction was removed using $Mg(NO_3)_2$ (Leleyter and Probst, 1999). The sequential extraction protocol is summarized in Table 1. All stock solutions were prepared with Millipore™ Milli-Q water (18.2 MΩ·cm at 25°C). Approximately 15 mg of sodium citrate per gram of sample were added to the sample at the beginning of each step of sequential extraction to minimize U and Th re-adsorption (Lozano et al., 2011; Martin et al., 2015). After each step, the solid residue was separated from the solution by centrifugation at 3500 rpm for 10 minutes and the supernatant was removed using a Pasteur pipette. The sequential extraction procedure was performed using the following reagents (with the grade and supplier in brackets): (i) the exchangeable fraction was extracted using 8 ml of 1M $Mg(NO_3)_2$ (magnesium nitrate, Suprapur, Merck) per gram of sample and agitated at 200 rpm on an orbital shaker at room temperature for 50 minutes. (ii) To extract carbonates the residue from step (i) was leached with 8 ml of 1M NaOAc (sodium acetate, Analytical grade, Merck) per gram of sample. The pH was adjusted to 5 using glacial HOAc (acetic acid, Reagent grade, ThermoFisher) and the solution was agitated at 200 rpm on an orbital shaker for 5 hr at room temperature. (iii) To eliminate Fe- and Mn- oxides, the residue from step (ii) was treated with 20 ml of 0.04M NH2OH·HCl (hydroxylamine hydrochloride, TraceSELECT>99.9999%, Sigma-Aldrich) in 25% (v/v) HOAc at 95°C for 6 hr and agitated manually every 30 minutes. Finally, (iv) the organic matter was leached from the residue of step (iii) with a three-stage leaching. Firstly, 3 ml of 0.02M HNO_3 and 5 ml of 30% H_2O_2 (Reagent grade, Merck) per gram of sample were added to the centrifuge tubes and the pH was adjusted to 2 with 69% HNO_3 (ACS Reagent grade, Merck). The solution was kept at room temperature for 1 hr, the temperature was then increased slowly to 85°C and left at the same temperature for 1.5 hr,

agitating manually every 30 minutes. Secondly, 3 ml of 30% H_2O_2 per gram of sample were added and the pH was adjusted to 2 with 69% HNO_3. The solution was heated at 85°C for 3 hr and agitated every 30 minutes. Finally, 5 ml of 3.2M NH_4OAc (ammonium acetate, TraceSELECT>99.9999%, Sigma-Aldrich) in 20% (v/v) HNO_3 per gram of sample were added and the total volume was taken up to 40 ml using Milli-Q water. The solution was agitated for 30 minutes on the orbital shaker at room temperature. At the end of the sequential extraction treatment an aliquot of about 100 mg was saved for U-series and major element analysis. This aliquot is referred to as *leached* throughout the article.

The etching procedure was performed on the leached samples. Twenty ml of 0.3M HF/ 0.1M HCl per gram of sample were added to the PFA centrifuge tube and agitated on the orbital shaker at 2000 rpm for 24 hr. An aliquot of about 100 mg of the solid residue was taken after 1, 2, 4, 8 and 24 hr. Each aliquot was transferred to a clean centrifuge tube and washed twice with 12 ml of Milli-Q water. Finally, all aliquots were dried in an oven at 70°C.

About 100 mg of each sample were spiked with ~30 mg of ^{229}Th-^{236}U tracer solution before acid dissolution. All reagents used during acid dissolution were Merck™ Suprapur grade. Samples were dissolved with 2.5 ml 48% HF and 0.5 ml 69% HNO_3 in 30 ml PFA vials at 100°C overnight. Dissolved sample solutions were dried to incipient dryness at 120°C. If dissolution was not fully completed, solutions were transferred to polytetrafluoroethylene (PTFE) digestion bombs and a mixture of 0.5 ml 69% HNO_3 and 1.5 ml concentrated 30% HCl was added. Bombs were heated at 200°C for more than 12 hr and then solutions were dried to incipient dryness at 120°C. The fully dissolved samples were then treated with 3 ml of 6M HCl. When necessary, H_3BO_3 was added to dissolve any residual fluorides. Solutions were heated at 80°C overnight and dried to incipient dryness at 100°C. Samples were then re-fluxed with 0.5 ml of 69% HNO_3 twice. Finally, samples were taken in 2 ml of 1.5 M HNO_3. The resulting solutions were than divided in two aliquots: a) 0.1 ml was saved for major element analysis; b) the remaining solution was used for U-Th separation. This was performed by ion exchange chromatography using 0.5 ml of TRU resin (Eichrom), following the protocol described in Luo et al. (1997). Uranium and Th elutions were dried to incipient dryness, taken in 0.5 ml of 31% H_2O_2 and dried down again. A drop of 69% HNO_3 was added, dried down and finally the sample was dissolved in 2% HNO_3 before U-series isotopic analyses.

The U-series isotopic analyses were performed using Sims (2008) procedure on a ThermoFisher Neptune Plus Multi-Collector Inductively Coupled Plasma-Mass Spectrometer

at the Research School of Earth Science, Australian National University. Certified Reference Material (CRM) U010 and synthetic standard OU Th'U' were used for sample bracketing for U and Th analysis, respectively. Synthetic standards U005-A and UCSC Th'A' were analysed as unknown solutions for U and Th, respectively and measurements were within 7‰ of the certified values (Richter et al., 2011; Rubin, 2001). Total procedure blanks were <53 pg for U and <214 pg for Th, while the average amounts of U and Th analysed in samples were 0.1 and 0.7 µg, respectively. Accuracy was assessed by analysing USGS QLO-1 rock standard and values were within error for U and Th concentrations (3.0% for U, 2.2% for Th) relative to certified values, whereas ($^{234}U/^{238}U$) and ($^{230}Th/^{238}U$) were within 0.4% and 6.5% of secular equilibrium (United States Geological Survey, 1995). The relatively poor accuracy on ($^{230}Th/^{238}U$) could be explained by heterogeneity of QLO-1. The external analytical error was estimated by sample replicates.

Magnesium (Mg), aluminium (Al), potassium (K), titanium (Ti), iron (Fe) and zirconium (Zr) concentration analyses were performed using an Agilent 7500 Series Inductively Coupled Plasma Mass Spectrometer (Q-ICP-MS) at University of Wollongong, Australia. Elemental concentrations were calculated by constructing a calibration curve from 12 standards, with concentration ranging from 0 to 500 ppb. The accuracy was determined analysing a gravimetric standard (QLO-1) and the relative deviations from recommended values (REF) were better than 2.4%, 11.3%, 6.3%, 6.5%, 1.5% and 4.8% for Mg, Al, K, Ti, Fe and Zr, respectively. For one gravimetric standard, K concentration was 30% within recommended value; this may be due to contamination occurred during sample preparation. Total procedure blanks contributed on the average amount of element analysed for less than 0.04%, 0.11%, 0.50%, 0.01%, 0.01%, 0.02% for Mg, Al, K, Ti, Fe and Zr respectively. External analytical uncertainties were calculated as the relative standard error of sample and gravimetric standard replicates (see Table 3).

The X-ray diffraction (XRD) measurements were undertaken on milled samples. Samples were mounted on holders and analysed with a Phillips 1130/90 diffractometer set to 35 kV and 28.8 mA. A Spellman DF3 generator was set to 1 kW and samples were analysed using an automatic sample holder. The analysis were performed with 2-theta values between 4 and 70° at 2° per minute and a step size of 0.02. The data were then processed through GBC 122 control system, and Traces and SIROQUANT softwares. The accuracy obtained by XRD routine analysis is normally about ± 3% at the 95% confidence level (e.g. Hillier, 2000). Loss on Ignition was

266 determined on approximately 2 grams of sample. The sample was placed in a furnace at 550°C
267 for 4 hr, using the methodology recommended by Heiri et al. (2001).

268 3. Results and discussion

269 The XRD mineralogy data and major elements concentrations are presented in Table 2 and 3.
270 We first identified an immobile element and used it to estimate relative gains and losses of
271 other elements.

272 3.1 Titanium as a immobile element

273 Titanium and zirconium are relatively immobile in regolith during weathering (Brimhall et al.,
274 1992; Neaman et al., 2004; Pelt et al., 2008). Several observations suggest that Ti is immobile
275 in our weathering profile. Firstly, untreated samples show increasing TiO_2 content with
276 decreasing depth. Secondly, the linear relationship between Zr and TiO_2 concentrations
277 (R^2=0.57; Figure 1) for untreated, leached and etched samples implies that they are not
278 significantly mobilized during the experiment. Alternatively, the two elements could be
279 mobilized at a similar rate throughout the weathering profile and during sequential extraction
280 and etching, which is unlikely. Finally, the Zr/TiO_2 ratios in untreated bedrock, saprolite and
281 soil remain relatively constant throughout the profile (relative standard deviation, RSD, <
282 ±20%). We chose Ti as the least mobile element because the Zr/TiO_2 ratios slightly decrease
283 during sequential extraction and etching, indicating a possible loss of Zr.

284 3.2 Bedrock

285 Analysis of a thin section of the untreated bedrock showed microphenocrysts of olivine and
286 plagioclase, cemented together by a fine glass matrix. The XRD data confirmed that the
287 untreated bedrock is composed largely of olivine, pyroxene, plagioclase and K-feldspar, and
288 minor concentrations of magnetite and hornblende. While the ($^{234}U/^{238}U$) activity ratio was in
289 secular equilibrium, the ($^{230}Th/^{238}U$) was lower than 1. This is surprising as the untreated
290 bedrock is expected to be in secular equilibrium for both radioactive systems. It is possible that
291 ^{230}Th is preferentially removed relative to ^{238}U during incipient dissolution. The preferential
292 loss of Th over U during rock dissolution is supported by the experiments of Tilton et al. (1955)
293 who observed that a greater fraction of labile Th relative to U was removed during a 5-minute
294 acid stirring of ground rocks. The authors suggested that a large amount of mobile U and Th is
295 present in mineral fractures and interstices and are therefore easily mobilized during incipient
296 rock dissolution. Enrichment in ^{238}U relative to ^{230}Th in slightly weathered bedrocks was also

observed by Pelt et al. (2008) and Dosseto et al. (2012).This occurrence could be explained by the fact that ^{230}Th is produced by alpha-decay resulting in the nuclide being located in recoil tracks from which it can be easily mobilized by solutions (Gögen and Wagner, 2000; Kigoshi, 1971; Murakami et al., 1991). Hence, during incipient weathering, ^{230}Th may be preferentially mobilized relative to ^{238}U, which may be retained in primary minerals.

Following sequential extraction, we observed a loss of Mg, K, Fe and Al relative to Ti (Fig. 2), while XRD data indicated loss of olivine. Olivine dissolution explains the losses of Mg and Fe, while other labile phases in basaltic rocks are glass and inter-granular phases (Chesworth et al., 1981; Chesworth et al., 2004; Eggleton et al., 1987; Tieh et al., 1980). Glass commonly concentrates K and Al (e.g. Karrat et al., 1998) and can explain the loss of these elements from the bedrock. However, XRD cannot detect glass and inter-granular phases as their structure is amorphous. Despite sequential extraction having been designed to remove solution-derived phases and organic matter (Tessier et al., 1979), some of the steps are performed at low pH and temperatures up to 96°C for several hours, which could be conditions aggressive enough to dissolve glass and olivine. For instance, glass dissolution experiments have been performed at pH 3 (e.g. Möller and Giese, 1997; Oelkers and Gislason, 2001). Similarly, studies have carried out dissolution experiments of olivine at temperatures between 25 and 65 °C, and pH between 2 and 5 (Chen and Brantley, 2000; Valsami-Jones et al., 1998). In natural environments, Chesworth et al. (1981) observed results similar to our laboratory experiments. They studied the evolution of the elemental composition of a basaltic profile and suggested rapid dissolution of glass and olivine from the unweathered rock, associated with losses of Mg, Na and K during early stages of weathering. The authors concluded that when labile phases are completely dissolved, the release of Mg and K reduces, indicating the presence of residual, more resistant minerals such as plagioclases and pyroxenes.

Following sequential extraction, we observe a loss of U and Th (Fig. 3) probably due to the dissolution of glass and inter-granular phases. Sequential extraction resulted in the removal of ~72% and ~64% of U and Th relative to Ti from the bedrock. These losses suggest dissolution of one or several labile, U- and Th-bearing phases. As discussed above, the phases most likely dissolved during sequential extraction are olivine and glass, but large amount of U and Th could also be retained in unstable inter-granular phases (Tieh et al., 1980). Olivine usually contains very low U and Th (Harmon and Rosholt, 1982), in contrast with glass (Dostal and Capedri, 1975; Dostal et al., 1976). Glass concentrates U and Th because of the incompatibility of these elements during magma differentiation (Hofmann, 1988). If we consider a bedrock

with 1 ppm of U and 22 wt.% of olivine, and assuming a U concentration in olivine of 0.01 ppm (Harmon and Rosholt, 1982), the olivine would contribute only ~0.22% of the total U present in the bedrock. This suggests that this mineral is unlikely to be responsible for the observed loss of U following sequential extraction. In contrast, glass contents in basalt are commonly of the order of 10 wt.% (Robertson and Peck, 1974), and reported U concentrations in glass are between 0.2 and 11 ppm (Aumento, 1971; Walton et al., 1981). Assuming glass concentration in our basalt of 10 wt.%, containing 2 ppm of U, the glass would contribute 20% of the total U budget in the bedrock. The remaining fraction of U lost may be supplied by inter-granular phases. Uranium in inter-granular phases could be released due to the experimental conditions applied during sequential extraction. For instance, Tilton et al. (1955) found that 34 and 42% of U and Th were removed from inter-granular phases of a granitic bedrock by a 5-minutes stirring with 6 M HCl. This suggests that the dissolution of inter-granular phases can result in the large losses of U and Th .

After sequential extraction, the ($^{234}U/^{238}U$) activity ratio increased by ~1% and ($^{230}Th/^{238}U$) by ~40% (Fig. 4). The lack of significant variation in the ($^{234}U/^{238}U$) ratio may suggest that sequential extraction removes phases with isotopic composition similar to the bedrock. In contrast, the increase in ($^{230}Th/^{238}U$) is explained by the preferential loss of U over Th during glass dissolution and the removal of inter-granular U and Th. Thus, it is not recommended to perform sequential extraction on bedrock because primary phases can be lost and artefacts in ($^{230}Th/^{238}U$) introduced.

The XRD data suggested only a loss of olivine during etching, while the rest of the primary minerals remained unchanged (Table 2). We observed a loss of K and Al relative to Ti during the first hour of etching, while for longer duration their abundances remained relatively constant (Fig. 2). In contrast, Mg and Fe concentrations showed a slight, but continuous decrease during the 24 hr of etching. Whereas the continuous losses of Mg and Fe confirm olivine dissolution, K and Al suggest that glass is dissolved only during the first hour. After 1 hr of etching, it is possible that glass is no longer present in the residue or our methodology is not able to detect further losses. Thorium/titanium and U/Ti ratios did not significantly change. This indicates that etching removes phases with no or low concentrations of U and Th. This is supported by the observed dissolution of olivine.

During etching, ($^{234}U/^{238}U$) and ($^{230}Th/^{238}U$) activity ratios increased continuously relatively to the leached bedrock, showing values greater than one (Fig. 4). This is unexpected, because

during mineral dissolution ^{234}U is thought to be more mobile than ^{238}U and weathering products are expected to show ($^{234}U/^{238}U$) <1 (e.g. Chabaux et al., 2003; Dequincey et al., 2002; Dosseto et al., 2008a; Ma et al., 2010). Therefore, the increase in ($^{234}U/^{238}U$) indicates that phases depleted in ^{234}U relative to ^{238}U are removed. Several authors have reported the removal of phases depleted in ^{234}U relative to ^{238}U during acid-leaching experiments (Essien, 1990; Romer and Rocholl, 2004; Sheng and Kuroda, 1986b; Shirvington, 1983). For instance, Sheng and Kuroda (1986a) performed acid leaching experiments on carnotite and observed ($^{234}U/^{238}U$) >1 in the residue. They suggested that ^{234}U is recoiled from a labile, U-rich phase to an adjacent resistant, U-poor phase (*Sheng-Kuroda effect*). As a result, the resistant, U-poor phase becomes enriched in ^{234}U with respect to ^{238}U, while the labile, U-poor phase becomes depleted in the same isotope. During dissolution, if the U-rich phase is preferentially removed, the residue will be enriched in ^{234}U relative to ^{238}U. This mechanism is mainly influenced by two factors. Firstly, the larger the difference in U contents between the two adjacent phases, the more effective the transfer of the radiogenic nuclides is (Sheng, 1986; Sheng and Kuroda, 1986a). Secondly, the size of the U-poor mineral relative to the ^{234}Th α-recoil range, that is 55 nm (Kigoshi, 1971), must be small enough to produce a measurable isotopic fractionation. Recently Tanaka et al. (2015) performed a one-step acid leaching on powdered basaltic rocks, and obtained results similar to ours. The authors concluded that the ($^{234}U/^{238}U$) and ($^{230}Th/^{238}U$) above unity observed in the acid-leaching residue was the result of alpha-recoil of ^{234}U and ^{230}Th from labile to resistant phases in the groundmass. In our study the labile U-rich phase is most likely glass, while resistant U-poor phases are fine-grained feldspars and pyroxene present in the groundmass. Therefore, ^{234}U and ^{230}Th recoiled from glass into fine-grained feldspars and/or pyroxenes would result in ($^{234}U/^{238}U$) and ($^{230}Th/^{238}U$) <1 in glass, and the opposite in feldspar and pyroxene During etching, as glass may be dissolving faster than pyroxene and feldspar (Chesworth et al., 2004), this could account for increasing ($^{234}U/^{238}U$) and ($^{230}Th/^{238}U$) activity ratios. In addition, as the ^{234}U previously implanted into feldspar and pyroxene decays into ^{230}Th, this could produce further enrichment in ^{230}Th and account for ($^{230}Th/^{238}U$) ratios greater than ($^{234}U/^{238}U$).

3.3 Saprolite

By comparing untreated bedrock and saprolite we aimed at investigating the effects of the conversion of bedrock into saprolite on the mineralogy, major element and U-series isotopic composition of the regolith. The XRD data showed that the untreated saprolite had a lower olivine, plagioclase, K-feldspar and pyroxene content, compared to the untreated bedrock, while a significant abundance of clay minerals was present (Table 2).

The MgO/TiO_2 and K_2O/TiO_2 ratios were lower in the saprolite compared to the bedrock, indicating a loss of Mg and K during the conversion of the bedrock into saprolite. In contrast, Al_2O_3/TiO_2, Fe_2O_3/TiO_2, U/TiO_2 and Th/TiO_2 ratios and the ($^{234}U/^{238}U$) and ($^{230}Th/^{238}U$) activity ratios remained almost unchanged (Fig. 5 and 6). The loss of Mg and K is explained by the weathering of olivine and K-feldspar, respectively. Because olivine and glass have similar susceptibility to weathering, it is likely that glass is also dissolved (Eggleton et al., 1987). As we observe a loss of Al- and Fe-bearing minerals (feldspars, pyroxenes and olivine), the constant Al_2O_3/TiO_2 and Fe_2O_3/TiO_2 could be explained by the in-situ conversion of these phases into secondary phases, i.e. bedrock-derived clays. In principle, weathering of silicate minerals is mostly driven by hydrolysis reactions (Trescases et al., 1992), in which cations located in the mineral lattice are replaced by hydrogen ions from solution. During these processes mobile elements, such as Mg and K, are removed, while less mobile elements, such as Al and Fe, remain and recombine to form clays (Arslan et al., 2006). For instance, weathering of olivine initially results in the formation of Fe-oxides and hydrated Mg-silicate. Successively, Mg is lost while Fe remains; the latter recombines with SiO_4 tetrahedra to form, depending on the weathering conditions, smectite, montmorillonite, hematite and/or goethite (Delvigne et al., 1979). Similarly, feldspar commonly weather to kaolinite, secondary mica (e.g. sericite) and/or allophane (Ollier and Pain, 1996) and glass into Fe-rich kaolinite (Arslan et al., 2006).

The constant U/TiO_2 and Th/TiO_2 ratios between the untreated bedrock and saprolite imply that there is no loss of U and Th during clay formation. Similarly, the ($^{234}U/^{238}U$) and ($^{230}Th/^{238}U$) activity ratios showed similar values, confirming that these nuclides are not considerably lost during clay formation. Note that the estimation of regolith production rates is based on the fractionation among the U-series isotopes. Therefore, because U and Th are not fractionated during the conversion of primary minerals into clays, the latter phases need to be preserved.

The untreated saprolite was sieved at 125 µm and the coarser fraction was retained. The fraction coarser than 125µm displayed MgO/TiO_2 and Fe_2O_3/TiO_2 ratios similar to those of the untreated saprolite, but higher K_2O/TiO_2 and Al_2O_3/TiO_2 ratios (Fig. 7). The gain in K and Al may suggest that the coarser size fraction is enriched in K-feldspars. Sieving had little effect on the U and Th concentrations and activity ratios. This suggests that U and Th isotopes are uniformly distributed across these size fractions. The higher U/TiO_2 value in the coarse fraction of the lower saprolite may be an analytical artefact (Fig. 8); the U concentration was anomalously high compared to all other samples, while TiO_2 concentration was similar. The grain-size fraction coarser than 125 µm was used for sequential extraction and etching, as described in the method section.

Following sequential extraction, there is no evidence for a loss of primary minerals but clay contents decreased by ~30 and ~12% in the lower and upper saprolite, respectively. Note that the decrease in clays is likely to represent the combined effect of sequential extraction and sieving. It was not possible to differentiate between the two, considering that we were unable to undertake XRD analysis on sieved samples. Following sequential extraction of the saprolite, Mg, K, Al, U, and to a lesser extent Th were lost (Figs. 7 and 8). This is likely to be explained by the loss of clays and possibly other phases such as Fe-oxides, during this treatment.

Sequential extraction had opposing effects on the ($^{234}U/^{238}U$) activity ratios of the upper and lower saprolites (Fig. 9). In the lower saprolite, it resulted in a decrease of the ($^{234}U/^{238}U$) activity ratio to a value below 1. This indicates the removal of phases with ($^{234}U/^{238}U$) >1, possibly bedrock-derived clays as suggested by XRD and major element data. As shown above, untreated bedrock and saprolite showed similar ($^{234}U/^{238}U$). This was explained as the absence of nuclide mobility during clay formation, possibly implying that clays have a ($^{234}U/^{238}U$) = 1. If this was the case, we should not observe a change in ($^{234}U/^{238}U$) following the loss of clays during sequential extraction. To explain this discrepancy, it is possible that clays have variable ($^{234}U/^{238}U$) activity ratios depending on which primary minerals they are derived from. In the previous section, we saw that pyroxenes and feldspars could be enriched in ^{234}U relative to ^{238}U as a result of Sheng-Kuroda effect. If the transformation of these minerals into clays occurred without loss or gain of nuclides, this would result in clays with ($^{234}U/^{238}U$) >1. Thus, the loss of these clays during sequential extraction would account for the observed ($^{234}U/^{238}U$) <1 in the residue.

In the upper saprolite, sequential extraction resulted in an increase in ($^{234}U/^{238}U$) to values greater than 1. This could be explained by the loss of clays with ($^{234}U/^{238}U$) <1. In the previous section, we proposed that glass could be characterised by a ($^{234}U/^{238}U$) <1 as a result of the Sheng-Kuroda effect. Hence, clays produced by alteration of glass could inherit a ($^{234}U/^{238}U$) <1. Their loss during sequential extraction of the upper saprolite could explain the observed ($^{234}U/^{238}U$) >1 in the residue.

Sequential extraction resulted in an increase of the ($^{230}Th/^{238}U$) activity ratios in both saprolites (Fig. 9). This suggests a preferential loss of U over Th during the removal of clays. This also indicates that residual phases present in the leached saprolite are characterised by a ($^{230}Th/^{238}U$) >1. This is consistent with the bedrock experiment, which showed that residual primary minerals at the end of sequential extraction and etching have a ($^{230}Th/^{238}U$) >1.

During etching, there is no evidence for any systematic variation in mineralogy. In both saprolites, there was no change in Fe_2O_3/TiO_2 and K_2O/TiO_2 ratios. In the lower saprolite, Al_2O_3/TiO_2 and MgO/TiO_2 ratios both increased and decreased during treatment, respectively. In the upper saprolite, these two ratios were continuously lost. This could be the result of minor loss of primary minerals, undetected by XRD, and/or of Al- and Mg-bearing poorly-crystalline phases (e.g. clays). While Th concentrations remained unchanged for both saprolites, U was lost during the first hour of etching (Fig. 8). Note that high U/TiO_2 and Th/TiO_2 ratios in the upper saprolite after 1 hr of etching are possibly due to anomalously low TiO_2 concentrations. The ($^{234}U/^{238}U$) and ($^{230}Th/^{238}U$) activity ratios increased during the first hour of etching to values above 1, and remained relatively constant for longer durations. These results indicate that one-hour etching removes phases containing Al, Mg and U, and with ($^{234}U/^{238}U$) and ($^{230}Th/^{238}U$) <1. This would produce a residue composed by resistant, bedrock-derived phases enriched in ^{234}U relative to ^{238}U, such as pyroxenes and feldspars. This hypothesis is supported by two observations: i) etching produces a residue with ($^{234}U/^{238}U$) and ($^{230}Th/^{238}U$) similar to the resistant primary minerals found in the bedrock after sequential extraction and etching (see Fig. 4); and ii) the increase in ($^{234}U/^{238}U$) occurs during the first hour of etching; this suggests the nearly complete removal of more labile phases (e.g. labile clays).

In summary, sequential extraction and etching may remove bedrock-derived phases, more specifically clays produced from weathering of primary minerals. Because solution-derived phases and organic matter are not present in the saprolite, in such a case sequential extraction and etching are not necessary.

3.4 Soil

When comparing untreated samples, the soil had lower olivine, pyroxene, plagioclase and clay contents than the saprolite (Tab. 2). Surprisingly, quartz was detected suggesting aeolian deposition is an important component of the soil mineral budget. This could also account for the lower abundance of other minerals, as a result of dilution by quartz input. Untreated soil shows a loss of Mg, gain of K compared to untreated saprolite, while Fe and Al remained nearly unchanged (Fig. 5). The immobility of Fe and Al in soil is similar to observations in untreated bedrock and saprolite. The loss of Mg could be explained by the dissolution of Mg-bearing phases such as olivine and clays. The gain in K could be accounted for by the aeolian deposition of K-rich phases along with quartz.

Untreated soils show a gain of U and Th when compared to the untreated saprolite (Fig. 5). It is also characterized by ($^{234}U/^{238}U$) >1 and ($^{230}Th/^{238}U$) <1 (Fig. 6). These values suggest a gain of ^{234}U and ^{230}Th, similarly to observations by Andersen et al. (2013) and Ma et al. (2010). This can be explained in two ways. Firstly, the gain of these nuclides could be related to their immobilization by organic matter, since LOI data show higher organic matter in the upper soil, compared to the saprolite (Table 3). In contrast, the concentration of organic matter in the lower soil is the same as the saprolite and it does not explain the addition of U and Th. Secondly, it is possible that solution-derived phases containing U, Th and K, but with low Al and Fe content, are precipitated into the soil from pore water. In both cases, organic matter and solution-derived phases are expected to show ($^{234}U/^{238}U$) >1 and ($^{230}Th/^{238}U$) <1 (Dequincey et al., 2002; Plater et al., 1992) and would explain the U-series isotopic composition of the soil.

The removal of the grain size fraction <125 µm resulted in an increase in K and Al contents relative to Ti, while Fe and Mg remained nearly unchanged (Fig. 10). This suggests that the grain size fraction < 125 µm is depleted in Al- and K-bearing phases, similarly to what was observed in the saprolite. The U concentrations and U-series activity ratios did not significantly change after sieving (Fig. 11 and 12). This suggests a homogeneous distribution of U-series isotopic composition across size fractions. Thus, aeolian inputs (concentrated in the fined-grained fraction) are unlikely to play a major role on the U-series isotope composition of this soil. For sequential extraction and etching, we retained the size fraction coarser than 125 µm.

After sequential extraction, there was no significant change in mineral abundances compared to the untreated soil (Table 2). However, we observed losses of Mg, K, Al, U and Th, while Fe remained unchanged (Fig. 10 and 11). Sequential extraction resulted in a decrease in

519 ($^{234}U/^{238}U$) from values greater to lower than 1, while the opposite was observed for
520 ($^{230}Th/^{238}U$) (Fig. 12). These results suggest that sequential extraction removes phases
521 containing Mg, K, Al, U and Th, with ($^{234}U/^{238}U$) >1 and ($^{230}Th/^{238}U$) <1. These could be
522 solution-derived phases and organic matter, which are expected to be characterised by
523 ($^{234}U/^{238}U$) >1 and ($^{230}Th/^{238}U$) <1.

524 During the 24 hr of etching, we observed a small increase in pyroxene and plagioclase contents,
525 associated with a small decrease in K-feldspar, while quartz and clays increased and decreased,
526 respectively. Aluminium abundance varied slightly, while Mg, K and Fe remained substantially
527 unchanged, relative to Ti. Titanium-normalised U and Th contents also showed little variations
528 during etching. Similarly, ($^{234}U/^{238}U$) and ($^{230}Th/^{238}U$) activity ratios remained mostly
529 unchanged. Therefore, etching does not remove phases containing U and Th. Major elements
530 and XRD data do not suggest mineral loss. Therefore, it seems that etching has little effect on
531 soil that has undergone sequential extraction. This suggests that sequential extraction
532 effectively removes solution-derived phases and organic matter, whereas etching has little to
533 no effect. Note that the presence of allochthonous quartz is unlikely to significantly affect the
534 U-series isotopic composition of the soil residue, because of its low content of U and Th.

535 In the soil, our results confirm the hypothesis formulated by Martin et al. (2015) and Lee
536 (2009). These authors suggested that in soil samples, solution-derived phases and organic
537 matter are expected to show ($^{234}U/^{238}U$) >1, whereas residual primary minerals (i.e. bedrock-
538 derived phases) should show an outer rind with ($^{234}U/^{238}U$) <1 and a core in secular equilibrium.
539 Sequential extraction and etching remove solution-derived phases and organic matter, and
540 decreases the ($^{234}U/^{238}U$) activity ratio of the residue to a minimum. The minimum ($^{234}U/^{238}U$)
541 activity ratio obtained during sequential extraction and etching represents the isotopic
542 composition of bedrock-derived phases in the regolith (Martin et al., 2015). Further etching
543 attacks the outer rind of bedrock-derived phases, which is depleted in ^{234}U relative to ^{238}U, and
544 results in increasing the ($^{234}U/^{238}U$) activity ratio toward 1. In our study, the minimum
545 ($^{234}U/^{238}U$) was reached after sequential extraction; hence we recommend applying this
546 treatment to soil in order to minimise the presence of solution-derived phases and organic
547 matter. Etching seems unnecessary as it results in little to no variation in the U-series isotopic
548 composition of leached soil.

4. Conclusions

We applied sequential extraction and mild HF/HCl etching to a bedrock, two saprolites and two soils of a basaltic weathering profile. The aim was to assess the effect of sequential extraction and etching on the U-series isotopic composition of regolith and to evaluate whether these processes can be used to minimize the role of solution-derived phases and organic matter on U-series isotopic ratios.

This study provides insights on the behaviour of U-series during regolith development. For instance, our results suggest that recoil of ^{234}U and ^{230}Th from U-rich, fine-grained phases and their implantation into adjacent minerals may be a fractionation process that is currently underestimated in U-series isotopic studies of regolith. More experiments are necessary to clarify the role played by this mechanism during the isotopic evolution of soil and saprolite.

The untreated bedrock was in secular equilibrium for ($^{234}U/^{238}U$) but not for ($^{230}Th/^{238}U$), indicating fractionation between ^{238}U and ^{230}Th during the early stages of water-rock interaction. The untreated saprolite showed activity ratios similar to the bedrock. We inferred that during the conversion of the bedrock into the saprolite olivine, feldspar, pyroxene and glass are converted into clays. During this process, the U-series isotopes are not significantly mobilized and show little to no fractionation. The untreated soil showed ($^{234}U/^{238}U$) >1 and ($^{230}Th/^{238}U$) <1; this reflects the presence of solution-derived phases and organic matter.

Overall, in basaltic weathering profiles where U-series isotope measurements are to be undertaken to derive regolith production rates, we recommend to i) use the untreated bedrock, ii) sieved saprolite (grain size fraction greater than 125 µm), and ii) apply the sequential extraction protocol summarized in Table 2 to sieved soil samples (grain size greater than 125 µm). The bedrock should not be treated, as there is no evidence for solution-derived or organic phases, and treatment mobilizes labile U and Th. The saprolite contains clays derived from the weathering of primary minerals. Because during the transformation of the bedrock into saprolite there is no evidence for U and Th added by solution, sequential extraction should not be performed on saprolite. In contrast, the soil contains solution-derived and organic phases; these phases need to be removed to expose the U-series isotopic composition of bedrock-derived phases. Our results suggest that this can be efficiently achieved with the sequential extraction protocol proposed. In contrast, mild HF/HCl etching does not affect the soil and thus seems unnecessary.

One could argue that different treatments would introduce artefacts in the estimates the U-series isotopic composition of the regolith profile. However, this study underlines that saprolite and soil are the result of different processes and thus contain phases of different origin; while soil shows evidences of solution-derived and organic phases, saprolite is mostly characterized by residual primary minerals and bedrock-derived clays. This study provides a promising, simple and cost-effective pre-treatment method to remove solution-derive phases and organic matter from regolith. It also emphasizes the importance of carefully evaluate the different effects of treatments on regolith. While this study does not intend to provide a single pre-treatment method suitable to all type of weathering profiles, conclusions should be applicable to similar basaltic profiles.

Acknowledgments

We would like to acknowledge an ARC Future Fellowship FT0990447 to AD and a University of Wollongong postgraduate scholarship award to DM. We thank Lili Yu, Helen Price and Allan Chivas for technical support with the Q-ICP-MS, Ashley Martin for useful and inspiring discussions and Brent Peterson for fieldwork assistance.

References

Andersen, M., Vance, D., Keech, A., Rickli, J., Hudson, G., 2013. Estimating U fluxes in a high-latitude, boreal post-glacial setting using U-series isotopes in soils and rivers. Chemical Geology 354, 22-32.

Andersen, M.B., Erel, Y., Bourdon, B., 2009. Experimental evidence for< sup> 234</sup> U–< sup> 238</sup> U fractionation during granite weathering with implications for< sup> 234</sup> U/< sup> 238</sup> U in natural waters. Geochimica et Cosmochimica Acta 73, 4124-4141.

Arslan, M., Kadir, S., Abdioğlu, E., Kolayli, H., 2006. Origin and formation of kaolin minerals in saprolite of Tertiary alkaline volcanic rocks, Eastern Pontides, NE Turkey. Clay Minerals 41, 597-617.

Aumento, F., 1971. Uranium content of mid-oceanic basalts. Earth and Planetary Science Letters 11, 90-94.

Blanco, P., Tomé, F.V., Lozano, J., 2004. Sequential extraction for radionuclide fractionation in soil samples: a comparative study. Applied radiation and isotopes 61, 345-350.

Blanco, P., Tomé, F.V., Lozano, J., 2005. Fractionation of natural radionuclides in soils from a uranium mineralized area in the south-west of Spain. Journal of environmental radioactivity 79, 315-330.

Brimhall, G.H., Chadwick, O.A., Lewis, C.J., Compston, W., Williams, I.S., Danti, K.J., Dietrich, W.E., Power, M.E., Hendricks, D., Bratt, J., 1992. Deformational mass transport and invasive processes in soil evolution. Science 255, 695-702.

Cattle, S.R., Mctainsh, G.H., Elias, S., 2009. Æolian dust deposition rates, particle-sizes and contributions to soils along a transect in semi-arid New South Wales, Australia. Sedimentology 56, 765-783.

Chabaux, F., Blaes, E., Stille, P., di Chiara Roupert, R., Pelt, E., Dosseto, A., Ma, L., Buss, H., Brantley, S., 2013. Regolith formation rate from U-series nuclides: Implications from the study of a spheroidal weathering profile in the Rio Icacos watershed (Puerto Rico). Geochimica et Cosmochimica Acta 100, 73-95.

Chabaux, F., Bourdon, B., Riotte, J., 2008. U-series geochemistry in weathering profiles, river waters and lakes. U/Th Series Radionuclides in Aquatic Systems, Radioactivity in the Environment 13, 49-104.

Chabaux, F., Riotte, J., Clauer, N., France-Lanord, C., 2001. Isotopic tracing of the dissolved U fluxes of Himalayan rivers: implications for present and past U budgets of the Ganges-Brahmaputra system. Geochimica et Cosmochimica Acta 65, 3201-3217.

Chabaux, F., Riotte, J., Dequincey, O., 2003. U-Th-Ra fractionation during weathering and river transport. Reviews in Mineralogy and geochemistry 52, 533.

Chen, Y., Brantley, S.L., 2000. Dissolution of forsteritic olivine at 65 C and 2< pH< 5. Chemical Geology 165, 267-281.

Chesworth, W., Dejou, J., Larroque, P., 1981. The weathering of basalt and relative mobilities of the major elements at Belbex, France. Geochimica et Cosmochimica Acta 45, 1235-1243.

Chesworth, W., Dejou, J., Larroque, P., Rodeja, E.G., 2004. Alteration of olivine in a basalt from central France. Catena 56, 21-30.

Delvigne, J., Bisdom, E., Sleeman, J., Stoops, G., 1979. Olivines, their pseudomorphs and secondary products. Stiboka.

Dequincey, O., Chabaux, F., Clauer, N., Sigmarsson, O., Liewig, N., Leprun, J.C., 2002. Chemical mobilizations in laterites: evidence from trace elements and 238U-234U-230Th disequilibria. Geochimica et cosmochimica acta 66, 1197-1210.

635 Dosseto, A., Bourdon, B., Turner, S., 2008a. Uranium-series isotopes in river materials: Insights into the
636 timescales of erosion and sediment transport. Earth and Planetary Science Letters 265, 1-17.

637 Dosseto, A., Buss, H., Suresh, P., 2011. The Delicate balance between soil production and erosion, and its role on
638 landscape evolution| Macquarie University ResearchOnline.

639 Dosseto, A., Buss, H.L., Suresh, P., 2012. Rapid regolith formation over volcanic bedrock and implications for
640 landscape evolution. Earth and Planetary Science Letters 337, 47-55.

641 Dosseto, A., Turner, S., Douglas, G., 2006. Uranium-series isotopes in colloids and suspended sediments:
642 timescale for sediment production and transport in the Murray–Darling River system. Earth and Planetary Science
643 Letters 246, 418-431.

644 Dosseto, A., Turner, S.P., Chappell, J., 2008b. The evolution of weathering profiles through time: New insights
645 from uranium-series isotopes. Earth and Planetary Science Letters 274, 359-371.

646 Dosseto, A., Turner, S.P., Chappell, J., 2008c. The evolution of weathering profiles through time: New insights
647 from uranium-series isotopes. Earth and Planetary Science Letters 274, 359-371.

648 Dostal, J., Capedri, S., 1975. Partition coefficients of uranium for some rock-forming minerals. Chemical Geology
649 15, 285-294.

650 Dostal, J., Capedri, S., Dupuy, C., 1976. Uranium and potassium in calc-alkaline volcanic rocks from Sardinia.
651 Lithos 9, 179-183.

652 Eggleton, R.A., Foudoulis, C., Varkevisser, D., 1987. Weathering of basalt: changes in rock chemistry and
653 mineralogy. Clays and Clay Minerals 35, 161-169.

654 Essien, I., 1990. Uranium isotope anomaly in minerals. Journal of Radioanalytical and Nuclear Chemistry 139,
655 331-337.

656 Gontier, A., Rihs, S., Chabaux, F., Lemarchand, D., Pelt, E., Turpault, M.-P., 2015. Lack of bedrock grain size
657 influence on the soil production rate. Geochimica et Cosmochimica Acta 166, 146-164.

658 Gögen, K., Wagner, G., 2000. Alpha-recoil track dating of Quaternary volcanics. Chemical Geology 166, 127-
659 137.

660 Handley, H.K., Turner, S.P., Dosseto, A., Haberlah, D., Afonso, J.C., 2013. Considerations for U-series dating of
661 sediments: Insights from the Flinders Ranges, South Australia. Chemical Geology 340, 40-48.

662 Harmon, R., Rosholt, J., 1982. Igneous rocks. Uranium Series Disequilibrium: Applications to Environmental
663 Problems (IVANOVICH, M., HARMON, RS, Eds), 145-166.

664 Heiri, O., Lotter, A.F., Lemcke, G., 2001. Loss on ignition as a method for estimating organic and carbonate
665 content in sediments: reproducibility and comparability of results. Journal of paleolimnology 25, 101-110.

666 Hillier, S., 2000. Accurate quantitative analysis of clay and other minerals in sandstones by XRD: comparison of
667 a Rietveld and a reference intensity ratio (RIR) method and the importance of sample preparation. Clay Minerals
668 35, 291-302.

669 Hofmann, A.W., 1988. Chemical differentiation of the Earth: the relationship between mantle, continental crust,
670 and oceanic crust. Earth and Planetary Science Letters 90, 297-314.

671 Karrat, L., Perruchot, A., Macaire, J.-J., 1998. Weathering of a Quaternary glass-rich basalt in Bakrit, Middle
672 Atlas Mountains, Morocco. Comparison with a glass-poor basalt. Geodinamica Acta 11, 205-215.

673 Kigoshi, K., 1971. Alpha-recoil thorium-234: dissolution into water and the uranium-234/uranium-238
674 disequilibrium in nature. Science 173, 47-48.

Lee, V.E., 2009. Radiogenic Isotope Geochemistry and the Evolution of the Earth's Surface and Interior. PhD Thesis.

Leleyter, L., Probst, J.-L., 1999. A New Sequential Extraction Procedure for the Speciation of Particulate Trace Elements in River Sediments. International Journal of Environmental Analytical Chemistry 73, 109-128.

Lozano, J., Blanco Rodríguez, P., Vera Tomé, F., Calvo, C.P., 2011. Enhancing uranium solubilization in soils by citrate, EDTA, and EDDS chelating amendments. Journal of hazardous materials 198, 224-231.

Luo, X., Rehkamper, M., Lee, D.-C., Halliday, A.N., 1997. High precision 230Th/232Th and 234U/238U measurements using energyfiltered ICP magnetic sector multiple collector mass spectrometry. International Journal of Mass Spectrometry and Ion Processes 171, 105-117.

Ma, L., Chabaux, F., Pelt, E., Blaes, E., Jin, L., Brantley, S., 2010. Regolith production rates calculated with uranium-series isotopes at Susquehanna/Shale Hills Critical Zone Observatory. Earth and Planetary Science Letters 297, 211-225.

Martin, A.N., Dosseto, A., Kinsley, L.P., 2015. Evaluating the removal of non-detrital matter from soils and sediment using uranium isotopes. Chemical Geology 396, 124-133.

Murakami, T., Chakoumakos, B.C., Ewing, R.C., Lumpkin, G.R., Weber, W.J., 1991. Alpha-decay event damage in zircon. American Mineralogist;(United States) 76.

Möller, P., Giese, U., 1997. Determination of easily accessible metal fractions in rocks by batch leaching with acid cation-exchange resin. Chemical geology 137, 41-55.

Neaman, A., Chorover, J., Brantley, S.L., 2004. Effects of organic ligands on granite dissolution in batch experiments at pH 6. American Journal of Science 306, 451-473.

Oelkers, E.H., Gislason, S.R., 2001. The mechanism, rates and consequences of basaltic glass dissolution: I. An experimental study of the dissolution rates of basaltic glass as a function of aqueous Al, Si and oxalic acid concentration at 25 C and pH= 3 and 11. Geochimica et Cosmochimica Acta 65, 3671-3681.

Ollier, C., Pain, C., 1996. Regolith, soils and landforms. John Wiley & Sons.

Pelt, E., Chabaux, F., Innocent, C., Navarre-Sitchler, A.K., Sak, P., Brantley, S.L., 2008. Uranium–thorium chronometry of weathering rinds: rock alteration rate and paleo-isotopic record of weathering fluids. Earth and Planetary Science Letters 276, 98-105.

Pelt, E., Chabaux, F., Stille, P., Innocent, C., Ghaleb, B., Girard, M., Guntzer, F., 2013. Atmospheric dust contribution to the budget of U-series nuclides in soils from the Mount Cameroon volcano. Chemical Geology.

Plater, A., Ivanovich, M., Dugdale, R., 1992. Uranium series disequilibrium in river sediments and waters: the significance of anomalous activity ratios. Applied Geochemistry 7, 101-110.

Rezzoug, S., Fernex, F., Michel, H., Barci-Funel, G., Barci, V., 2009. Behavior of uranium and thorium isotopes in soils of the Boréon area, Mercantour Massif (SE France): leaching and weathering rate modeling. Journal of radioanalytical and nuclear chemistry 279, 801-809.

Richter, S., Kühn, H., Aregbe, Y., Hedberg, M., Horta-Domenech, J., Mayer, K., Zuleger, E., Bürger, S., Boulyga, S., Köpf, A., 2011. Improvements in routine uranium isotope ratio measurements using the modified total evaporation method for multi-collector thermal ionization mass spectrometry. Journal of Analytical Atomic Spectrometry 26, 550-564.

Rihs, S., Prunier, J., Thien, B., Lemarchand, D., Pierret, M.-C., Chabaux, F., 2011. Using short-lived nuclides of the U-and Th-series to probe the kinetics of colloid migration in forested soils. Geochimica et Cosmochimica Acta 75, 7707-7724.

716 Robertson, E.C., Peck, D.L., 1974. Thermal conductivity of vesicular basalt from Hawaii. Journal of Geophysical
717 Research 79, 4875-4888.

718 Romer, R.L., Rocholl, A., 2004. Activity disequilibrium of< sup> 230</sup> Th,< sup> 234</sup> U, and< sup>
719 238</sup> U in old stilbite: Effects of young U mobility and α-recoil. Geochimica et Cosmochimica Acta 68,
720 4705-4719.

721 Rubin, K., 2001. Analysis of< sup> 232</sup> Th/< sup> 230</sup> Th in volcanic rocks: a comparison of
722 thermal ionization mass spectrometry and other methodologies. Chemical Geology 175, 723-750.

723 Schultz, M.K., Burnett, W.C., Inn, K.G., 1998. Evaluation of a sequential extraction method for determining
724 actinide fractionation in soils and sediments. Journal of Environmental Radioactivity 40, 155-174.

725 Sheng, Z., 1986. Further studies on the separation of acid residues with extremely high^< 234> U/^< 238> U
726 ratios from a Colorado carnotite. Radiochim. Acta 40, 95-102.

727 Sheng, Z., Kuroda, P., 1986a. Isotopic fractionation of uranium: Extremely high enrichments of 234U in the acid-
728 residues of a Colorado carnotite. Radiochim. Acta 39, 131-138.

729 Sheng, Z., Kuroda, P., 1986b. Isotopic fractionation of uranium: Extremely high enrichments of 234U in the acid-
730 residues of a Colorado carnotite. Radiochimca Acta 39, 131-138.

731 Shirvington, P., 1983. Fixation of radionuclides in the< sup> 238</sup> U decay series in the vicinity of
732 mineralized zones: 1. The Austatom Uranium Prospect, Northern Territory, Australia. Geochimica et
733 Cosmochimica Acta 47, 403-412.

734 Sims, K.W., Gill, J.B., Dosseto, A., Hoffmann, D.L., Lundstrom, C.C., Williams, R.W., Ball, L., Tollstrup, D.,
735 Turner, S., Prytulak, J., 2008. An inter-laboratory assessment of the thorium isotopic composition of synthetic and
736 rock reference materials. Geostandards and Geoanalytical Research 32, 65-91.

737 Suresh, P., Dosseto, A., Handley, H., Hesse, P., 2014. Assessment of a sequential phase extraction procedure for
738 uranium-series isotope analysis of soils and sediments. Applied Radiation and Isotopes 83, 47-55.

739 Suresh, P., Dosseto, A., Hesse, P., Handley, H., 2013. Soil formation rates determined from Uranium-series
740 isotope disequilibria in soil profiles from the southeastern Australian highlands. Earth and Planetary Science
741 Letters 379, 26-37.

742 Tanaka, R., Yokoyama, T., Kitagawa, H., Tesfaye, D.B., Nakamura, E., 2015. Evaluation of the applicability of
743 acid leaching for the 238 U–230 Th internal isochron method. Chemical Geology.

744 Tessier, A., Campbell, P.G., Bisson, M., 1979. Sequential extraction procedure for the speciation of particulate
745 trace metals. Analytical chemistry 51, 844-851.

746 Tieh, T.T., Ledger, E.B., Rowe, M.W., 1980. Release of uranium from granitic rocks during in situ weathering
747 and initial erosion (central Texas). Chemical Geology 29, 227-248.

748 Tilton, G.R., Patterson, C., Brown, H., Inghram, M., Hayden, R., Hess, D., Larsen, E., 1955. Isotopic composition
749 and distribution of lead, uranium, and thorium in a Precambrian granite. Geological Society of America Bulletin
750 66, 1131-1148.

751 Trescases, J., Butt, C., Zeegers, H., 1992. Chemical weathering. Regolith exploration geochemistry in tropical
752 and subtropical terrains.. 25-40.

753 United States Geological Survey, 1995. Certificate of Analysis, Quartz Latite, QLO-1.

754 Valsami-Jones, E., Ragnarsdottir, K., Putnis, A.a.a., Bosbach, D., Kemp, A., Cressey, G., 1998. The dissolution
755 of apatite in the presence of aqueous metal cations at pH 2–7. Chemical Geology 151, 215-233.

Vigier, N., Bourdon, B., Turner, S., Allègre, C.J., 2001. Erosion timescales derived from U-decay series measurements in rivers. Earth and Planetary Science Letters 193, 549-563.

Walton, A.W., Galloway, W.E., Henry, C.D., 1981. Release of uranium from volcanic glass in sedimentary sequences; an analysis of two systems. Economic Geology 76, 69-88.

Wellman, P., McDougall, I., 1974. Potassium-argon ages on the Cainozoic volcanic rocks of New South Wales. Journal of the Geological Society of Australia 21, 247-272.

Young, R.W., 1982. Soils of the Illawarra region. Wollongong Studies in Geography, 10.

Tables and figures

Table 1. Sequential extraction procedure used in this study and target phases. All reagent volumes are intended for 1 g of sample.

Phase aimed at	Procedure
(1) Exchangeable	8 mL of 1 M Mg(NO3)2. Agitate at room temperature for 50 min.
(2) Carbonates	16 mL of 1 M NaOAc at pH 5 (adjusted with AcOH). Agitated at room temperature for 5 hr.
(3) Fe- and Mn -oxides	20 mL 0.04M NH2OH·HCl/AcOH (pH 2). At 96 °C for 5 hr and agitated occasionally.
(5) Organic matter	- 3 mL of 0.02 M HNO3 + 5 mL 30% H2O2 at pH 2 (adjusted with HNO3), at 85 °C for 2 hrand occasionally agitated. - 3 mL 30% H2O2, pH 2 (adjusted with HNO3), at 85 °C for 3 hr and occasionally agitated. - 5 mL of 3.2 M NH4OAc in 20% HNO3, diluted up to 20 mL with H2O, agitated at room temperature for 30 min.

772

773 **Table 2. Mineralogical abundances (in wt.%) determined by X-ray diffraction.**

Sample name	Olivine	Pyroxene	Plagioclase	K-feldspar	Quartz	Clays	Hematite	Others	TOTAL
BR Untreated	22	16	47	12				4	100
BR Leached	14	15	55	12				4	100
BR 24h etching	6	20	51	16				7	100
C_{LOW} Untreated	6	5	12	4		69		5	100
C_{LOW} Leached	5	6	13	5		49		21	100
C_{UP} Untreated	8	5	14	8	1	58	3	5	100
C_{UP} Leached	8	6	13	11		51	3	9	100
C_{UP} 1h etching	8	6	14	9		52	2	9	100
C_{UP} 2h etching	7	6	12	9		58	2	6	100
C_{UP} 4h etching	8	4	13	11		53	3	9	100
C_{UP} 8h etching	9	5	12	10		47	4	14	100
C_{UP} 24h etching	7	5	10	12		54	3	8	100
S_{LOW} Untreated	4	4	9	5	21	40	4	13	100
S_{LOW} Leached	4	3	8	5	18	46	4	13	100
S_{UP} Untreated	5	2	8	10	21	41	5	10	100
S_{UP} Leached	3	5	5	7	35	33	5	6	100
S_{UP} 1h etching	6	5	8	9	13	35	5	19	100
S_{UP} 2h etching	5	3	9	4	17	42	5	15	100
S_{UP} 4h etching	5	3	7	6	14	43	6	17	100
S_{UP} 8h etching	3		8	1	34	32	6	16	100
S_{UP} 24h etching	3	10	12	2	13	40	4	15	100

774 **The accuracy obtained by XRD routine analysis is normally about ± 3% at the 95% confidence level (e.g. Hillier,**
775 **2000). "Others" include zircon, xenotime, mica, allanite, epidote and hornblende, and are present in concentrations <**
776 **5 wt.%.**

777 **Table 3 Major and trace element concentrations.**

Sample name	MgO (wt.%)	RSD	Al_2O_3 (wt.%)	RSD	K_2O	RSD	TiO_2 (wt.%)	RSD	Fe_2O_3T (wt.%)	RSD	Zr (ppm)	RSD	LOI (wt.%)
BR Untreated	10.00	0.72	14.49	6.10	0.84	6.74	1.72	1.06	11.91	4.72	215.42	1.53	1.3
BR Leached	12.03	1.24	20.11	0.55	1.45	4.89	3.70	1.01	18.87	2.76	431.96	0.78	
BR 1h etching	7.03	0.12	6.57	1.55	0.59	1.25	1.77	0.38	11.44	0.71	180.58	0.54	
BR 2h etching	5.09	0.44	7.80	1.33	0.60	1.20	1.78	1.29	9.72	0.39	190.97	0.88	
BR 24h etching	5.93	0.82	12.72	0.88	0.92	2.41	2.54	1.37	9.87	0.85	217.34	0.97	
C_{LOW} Untreated	1.90	1.89	20.87	7.22	0.05	4.83	2.31	0.81	14.81	4.92	291.96	2.23	10.2
C_{LOW} >125 µm	1.86	2.88	28.85	4.96	0.16	35.33	2.23	0.74	14.57	0.88	351.88	1.19	
C_{LOW} Leached	1.05	0.86	24.76	0.70	0.04	2.84	2.38	0.35	13.55	1.34	309.06	0.52	
C_{LOW} 1h etching	1.18	0.63	25.81	1.14	0.04	2.88	2.69	0.77	15.26	1.84	239.71	1.05	
C_{LOW} 2h etching	1.61	1.10	28.77	1.45	0.04	2.55	2.28	1.30	14.67	1.86	226.77	0.85	
C_{LOW} 4h etching	1.18	1.00	22.53	0.70	0.03	3.37	1.95	0.70	13.06	0.85	187.15	0.08	
C_{LOW} 8h etching	1.43	0.93	26.74	0.35	0.04	2.86	2.35	1.61	15.74	1.51	216.16	4.84	
C_{LOW} 24h etching	1.10	0.26	17.07	0.36	0.04	1.64	4.09	0.66	17.59	3.60	220.74	0.34	
C_{UP} Untreated	1.28	1.01	20.03	8.24	0.06	6.47	3.03	0.43	17.96	5.50	349.56	1.03	10.9
C_{UP} >125 µm	1.28	3.54	28.81	6.51	0.13	34.05	3.07	0.63	17.59	0.76	417.66	1.47	
C_{UP} Leached	0.86	0.75	24.96	1.04	0.04	3.79	3.07	0.70	17.01	1.92	390.69	0.93	
C_{UP} 1h etching	0.26	1.06	7.30	1.07	0.01	2.84	1.00	0.86	5.43	1.15	77.70	1.20	
C_{UP} 2h etching	0.93	2.60	20.89	2.83	0.06	4.01	3.93	0.44	19.29	2.52	290.73	2.41	
C_{UP} 4h etching	0.92	1.91	21.24	1.82	0.06	4.31	3.50	0.57	18.88	2.19	264.66	0.84	
C_{UP} 4h etching replicate	1.02	1.67	21.19	2.08	0.04	3.40	2.70	0.38	16.62	2.13	218.35	1.82	
C_{UP} 8h etching	0.72	1.06	19.15	1.16	0.06	3.79	4.86	0.27	21.67	2.98	283.09	1.02	
C_{UP} 8h etching replicate	0.72	2.80	19.24	3.06	0.06	3.27	4.36	0.76	20.90	1.85	265.04	2.48	
C_{UP} 24h etching	0.63	0.86	14.66	0.53	0.05	4.17	5.53	1.22	21.95	3.04	273.23	0.23	

Continues

[Continues]

Sample name	MgO (wt.%)	RSD	Al_2O_3 (wt.%)	RSD	K_2O	RSD	TiO_2 (wt.%)	RSD	Fe_2O_3T (wt.%)	RSD	Zr (ppm)	RSD	LOI(%)
S_{LOW} Untreated	0.50	1.60	21.29	8.24	0.21	7.97	2.49	0.27	14.93	5.66	291.82	1.71	10.6
S_{LOW} >125 µm	0.59	3.28	29.15	3.26	0.26	6.63	2.36	0.28	14.56	0.74	338.36	2.28	
S_{LOW} Leached	0.64	0.75	25.57	1.04	0.38	3.17	4.61	1.08	25.93	2.60	603.86	0.92	
S_{LOW} 1h etching	0.44	0.97	24.13	0.95	0.21	3.09	2.86	1.13	16.24	2.21	286.37	0.59	
S_{LOW} 2h etching	0.48	1.57	25.04	1.21	0.26	3.64	3.19	1.29	20.60	2.26	309.42	0.84	
S_{LOW} 4h etching	0.40	0.56	14.92	0.62	0.22	3.13	3.23	1.10	17.47	1.47	314.15	3.29	
S_{LOW} 8h etching	0.33	1.39	22.49	1.59	0.21	3.39	3.20	1.82	16.98	2.01	310.17	0.99	
S_{LOW} 24h etching	0.37	0.88	17.66	0.97	0.22	4.96	3.21	0.95	17.55	1.56	321.84	1.25	
S_{UP} Untreated	0.37	0.50	16.51	7.22	0.21	7.55	2.68	0.76	14.26	4.55	284.11	0.61	17.7
S_{UP} >125 µm	0.42	3.70	21.88	3.48	0.32	19.71	2.69	0.88		0.99	333.57	1.15	
S_{UP} Leached	0.64	1.33	23.44	1.29	0.47	3.45	5.76	1.45	28.64	1.60	651.29	1.58	
S_{UP} 1h etching	0.25	1.55	10.28	1.93	0.20	3.10	2.58	1.27	59.15	3.44	299.17	1.86	
S_{UP} 2h etching	0.35	1.33	17.12	0.95	0.25	2.67	2.92	0.76	15.53	1.74	291.70	0.94	
S_{UP} 4h etching	0.42	1.46	15.59	0.98	0.30	4.56	3.28	0.52	17.77	2.57	316.91	1.27	
S_{UP} 8h etching	0.43	1.42	19.53	1.26	0.37	2.85	5.01	1.00	26.44	1.28	449.31	1.08	
S_{UP} 24h etching	0.23	1.47	6.51	1.20	0.28	4.54	4.44	0.86	210.22	2.59	370.63	1.36	
QLO-1	1.01	1.37	16.40	1.37	2.52	1.57	0.66	1.49	4.42	1.34	210.57	0.72	
QLO-1	1.02	1.99	14.36	8.80	3.83	7.54	0.62	1.09	4.36	6.06	176.10	1.33	
Estimated external relative analytical uncertainties (RSE)	±4.9%		±0.15%		±3.18%		±12.9%		±6.4%		±9.6%		

Errors are internal analytical uncertainties (RSD). The estimated external relative analytical uncertainties (SE) were calculated from replicate analysis of rock standards and samples. Loss on Ignition (LOI) was measured at 500°C.

780 **Table 4 Uranium-series isotope results.**

Sample name	U (ppm)	2SE	Th (ppm)	2SE	($^{234}U/^{238}U$)	2SE	($^{230}Th/^{238}U$)	2SE
BR Untreated	1.009	0.002	3.312	0.003	0.997	0.002	0.880	0.006
BR Leached	0.614	0.001	2.546	0.002	1.010	0.002	1.237	0.007
BR 1h etching	0.447	0.001	1.912	0.002	1.043	0.002	1.327	0.008
BR 2h etching	0.437	0.001	2.066	0.002	1.063	0.002	1.503	0.008
BR 24h etching	0.350	0.000	2.343	0.001	1.101	0.003	1.975	0.009
C_{LOW} Untreated	1.245	0.002	4.445	0.006	0.998	0.002	0.850	0.006
C_{LOW} >125 μm	2.548	0.012	4.875	0.005	0.990	0.003	0.488	0.005
C_{LOW} Leached	1.007	0.001	4.470	0.004	0.977	0.003	1.126	0.006
C_{LOW} 1h etching	0.586	0.001	4.718	0.004	1.017	0.002	2.025	0.014
C_{LOW} 2h etching	0.546	0.001	3.647	0.003	1.017	0.002	1.879	0.009
C_{LOW} 4h etching	0.528	0.001	3.646	0.007	1.016	0.002	1.939	0.014
C_{LOW} 8h etching	0.575	0.001	4.155	0.004	1.014	0.002	1.885	0.011
C_{LOW} 24h etching	0.744	0.001	6.341	0.008	0.998	0.002	2.124	0.013
C_{UP} Untreated	1.903	0.006	6.018	0.009	1.004	0.001	0.851	0.007
C_{UP} >125 μm	1.791	0.007	5.624	0.008	1.000	0.003	0.925	0.009
C_{UP} Leached	1.279	0.002	5.367	0.006	1.017	0.002	1.218	0.008
C_{UP} 1h etching	0.735	0.001	6.097	0.008	1.050	0.003	2.381	0.016
C_{UP} 2h etching	0.778	0.001	7.141	0.008	1.039	0.003	2.515	0.011
C_{UP} 4h etching	0.684	0.001	6.056	0.007	1.032	0.002	2.424	0.013
C_{UP} 4h etching replicate	0.687	0.001	5.316	0.007	1.037	0.001	2.252	0.011
C_{UP} 8h etching	0.731	0.001	7.950	0.008	1.043	0.002	2.825	0.013
C_{UP} 8h etching replicate	0.787	0.001	8.442	0.008	1.039	0.002	2.870	0.013
C_{UP} 24h etching	0.766	0.001	8.350	0.013	1.042	0.002	3.016	0.021

Continues

[Continues]

S_{LOW} Untreated	1.901	0.006	7.351	0.012	1.009	0.002	0.919	0.006
S_{LOW} >125 µm	1.848	0.008	7.393	0.011	1.009	0.003	1.005	0.009
S_{LOW} Leached	1.008	0.002	6.792	0.014	0.974	0.003	1.660	0.014
S_{LOW} 1h etching	1.022	0.002	7.232	0.009	0.976	0.002	1.762	0.011
S_{LOW} 2h etching	1.133	0.001	8.320	0.008	0.976	0.002	1.733	0.009
S_{LOW} 4h etching	1.081	0.002	7.610	0.009	0.976	0.003	1.774	0.012
S_{LOW} 8h etching	1.051	0.003	7.567	0.010	0.974	0.002	1.779	0.014
S_{LOW} 24h etching	1.269	0.002	9.041	0.014	0.962	0.002	1.750	0.012
S_{UP} Untreated	2.123	0.007	8.445	0.014	1.020	0.002	0.963	0.007
S_{UP} >125 µm	2.290	0.008	8.969	0.011	1.009	0.003	1.039	0.009
S_{UP} Leached	1.287	0.006	9.243	0.015	0.960	0.004	1.824	0.019
S_{UP} 1h etching	1.315	0.004	10.061	0.024	0.955	0.002	1.972	0.018
S_{UP} 2h etching	1.320	0.002	9.589	0.018	0.968	0.002	1.875	0.014
S_{UP} 4h etching	1.251	0.003	9.205	0.019	0.961	0.002	1.816	0.014
S_{UP} 8h etching	2.168	0.005	15.977	0.035	0.960	0.002	1.833	0.018
S_{UP} 24h etching	0.416	0.000	12.984	0.031	0.974	0.002	7.856	0.054
QLO-1	1.842	0.007	4.420	0.005	1.004	0.002	0.935	0.007
QLO-1	1.880	0.005	4.447	0.006	1.003	0.002	0.907	0.007
Estimated external relative analytical uncertainties (RSE)	±4.1%		±4.6%		±0.2%		±4.8%	

781

782 **Errors are internal analytical uncertainties (2SE). The estimated external relative analytical uncertainties (RSE) were calculated from replicate analysis of rock standards and**
783 **samples; the highest error is reported in this table and used as uncertainties for the error bars in next figures.**

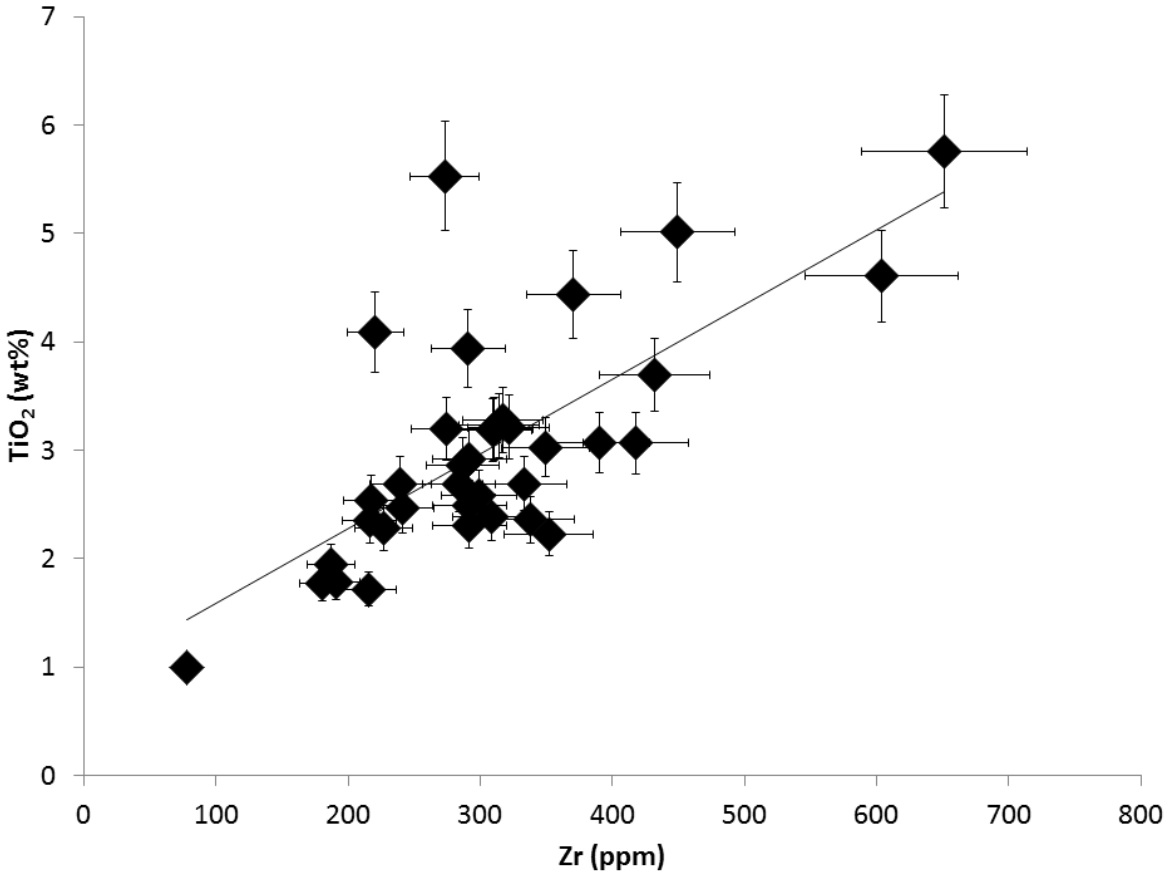

784

785 **Figure 1. Titanium oxide versus Zr concentrations for all samples of this study. The linear relationship shown has a**
786 **correlation coefficient, $R^2 = 0.5$.**

787

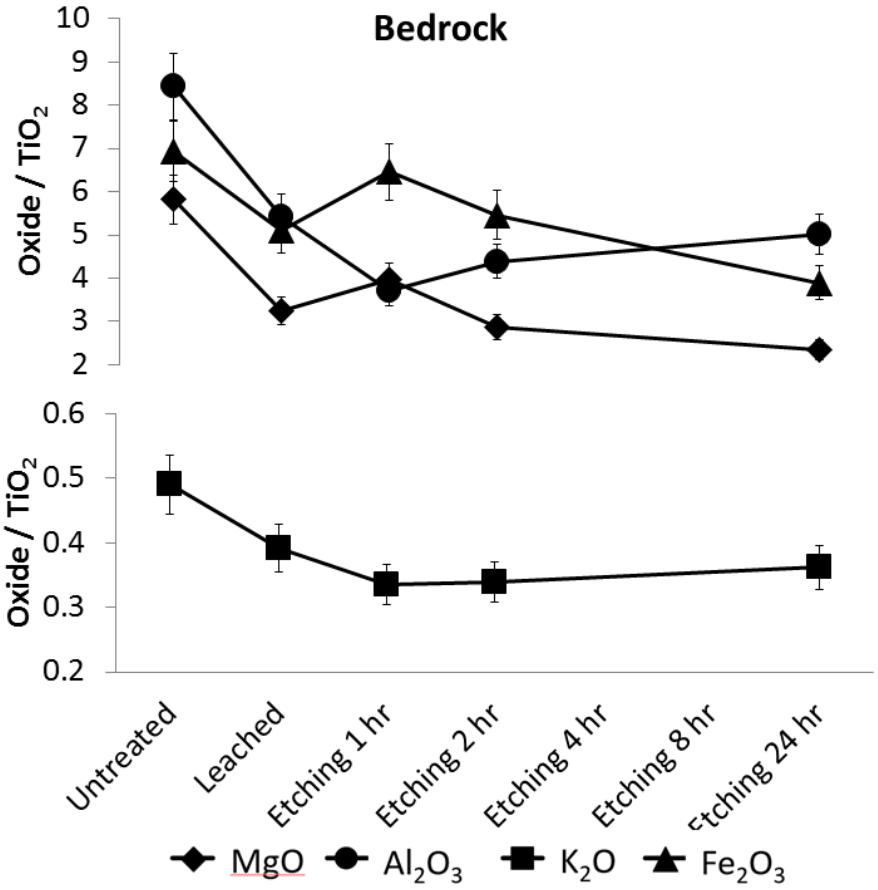

788

789 **Figure 2. Magnesium, K, Fe and Al oxides to TiO_2 ratios for untreated, leached and etched bedrock. Error bars**
790 **represent propagated external relative analytical uncertainties (RSE) reported in Tab. 2. In this figure and all the**
791 **following, error bars, if not shown, are within the symbol size.**

792

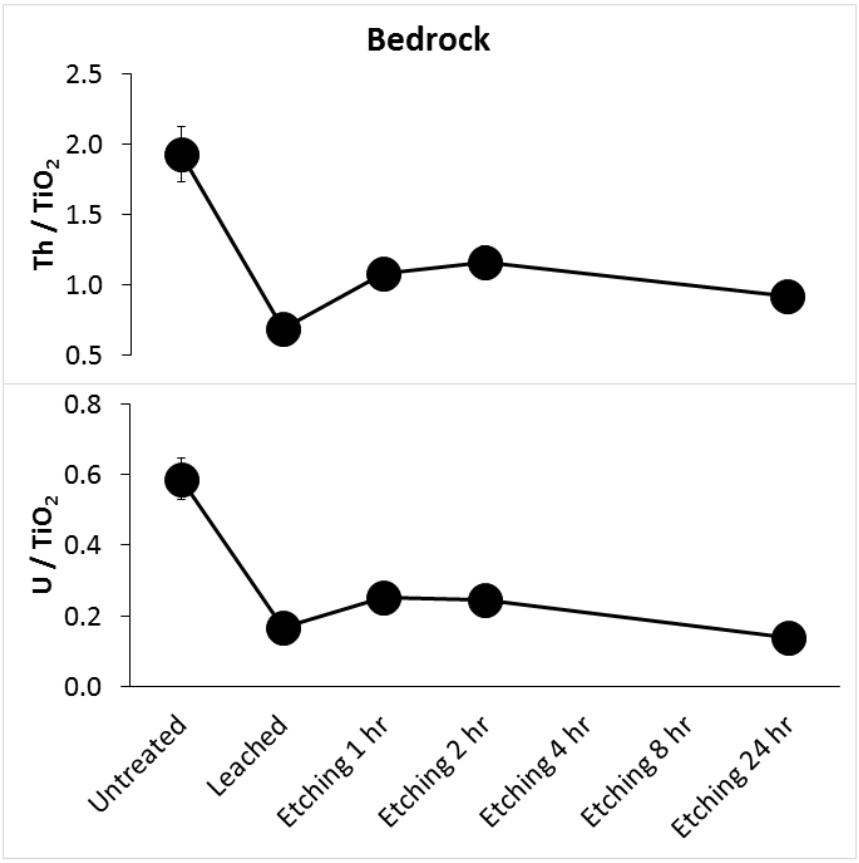

793

794 **Figure 3. Uranium and Th to TiO_2 ratios for the untreated, leached and etched bedrock. Error bars represent**
795 **propagated external relative analytical uncertainties (RSE) reported in Tab. 3.**

796

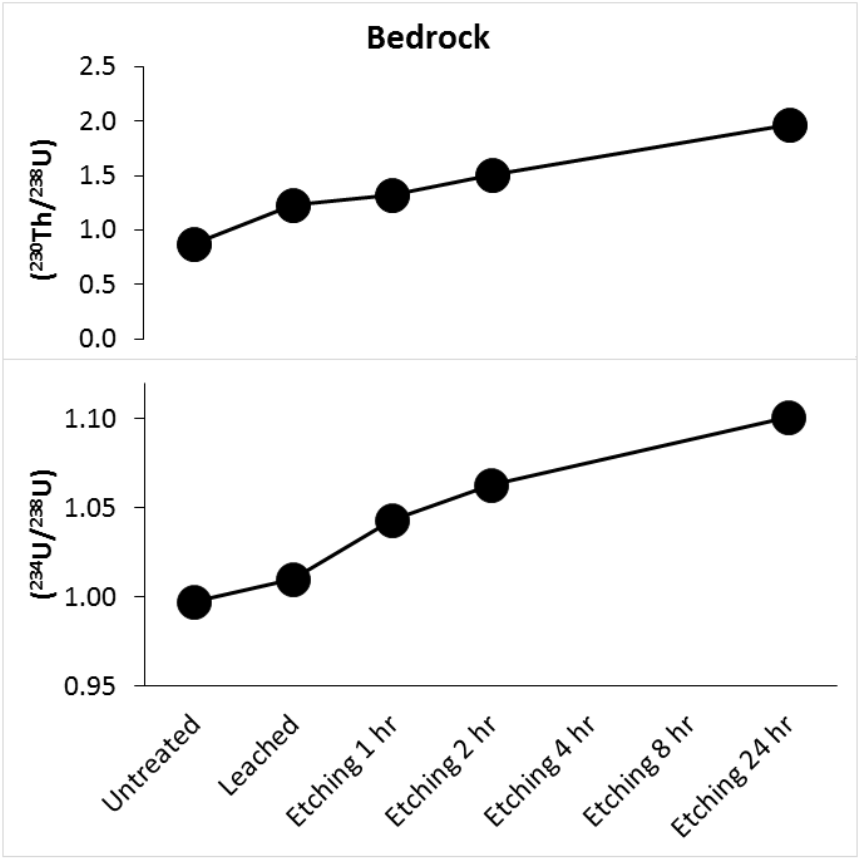

797

798 **Figure 4. ($^{230}Th/^{238}U$) and ($^{234}U/^{238}U$) for the untreated, leached and etched bedrock. Error bars represent external**
799 **relative analytical uncertainties (RSE) reported in Tab. 3.**

800

801

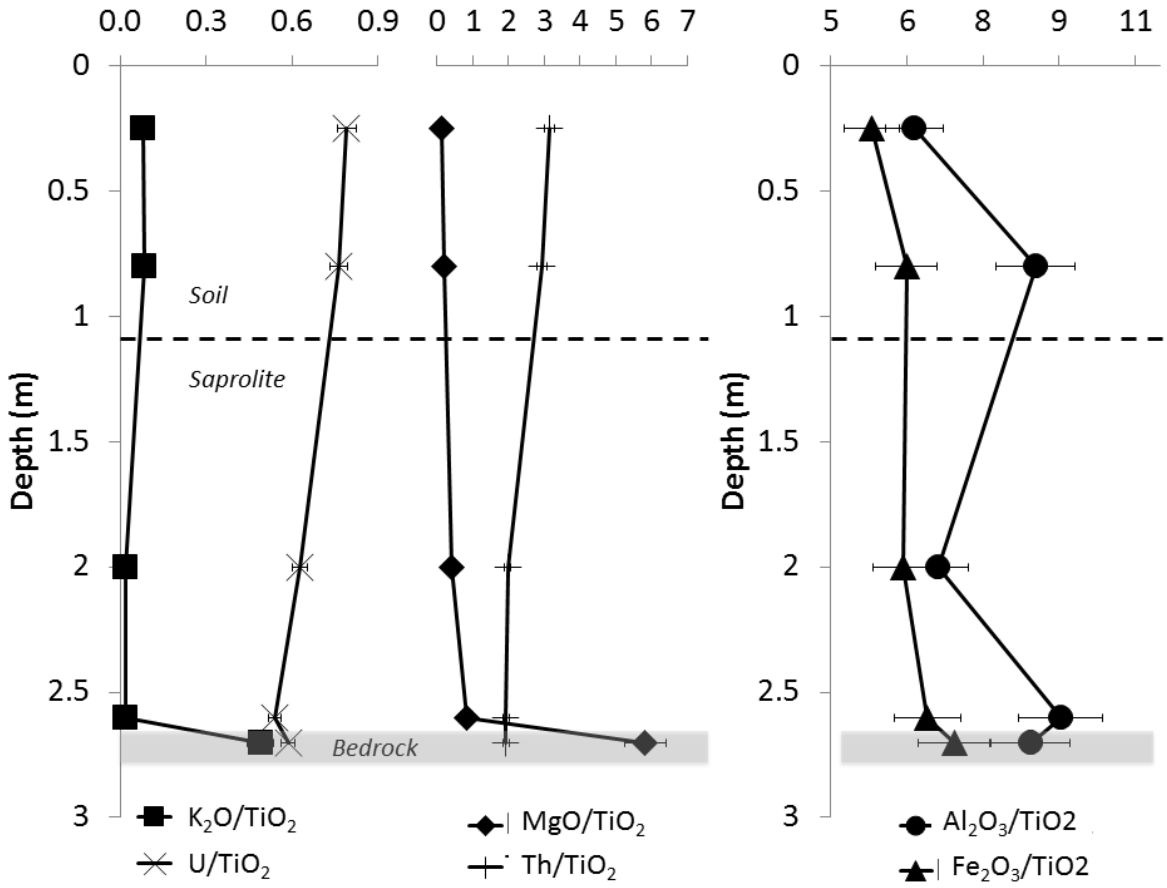

802

803 **Figure 5. Uranium, Th, MgO, Al_2O_3, K_2O and Fe_2O_3 to TiO_2 ratios as a function of depth, for untreated samples.**
804 **Error bars represent propagated external relative analytical uncertainties (RSE) reported in Table. 3.**

805

806

807

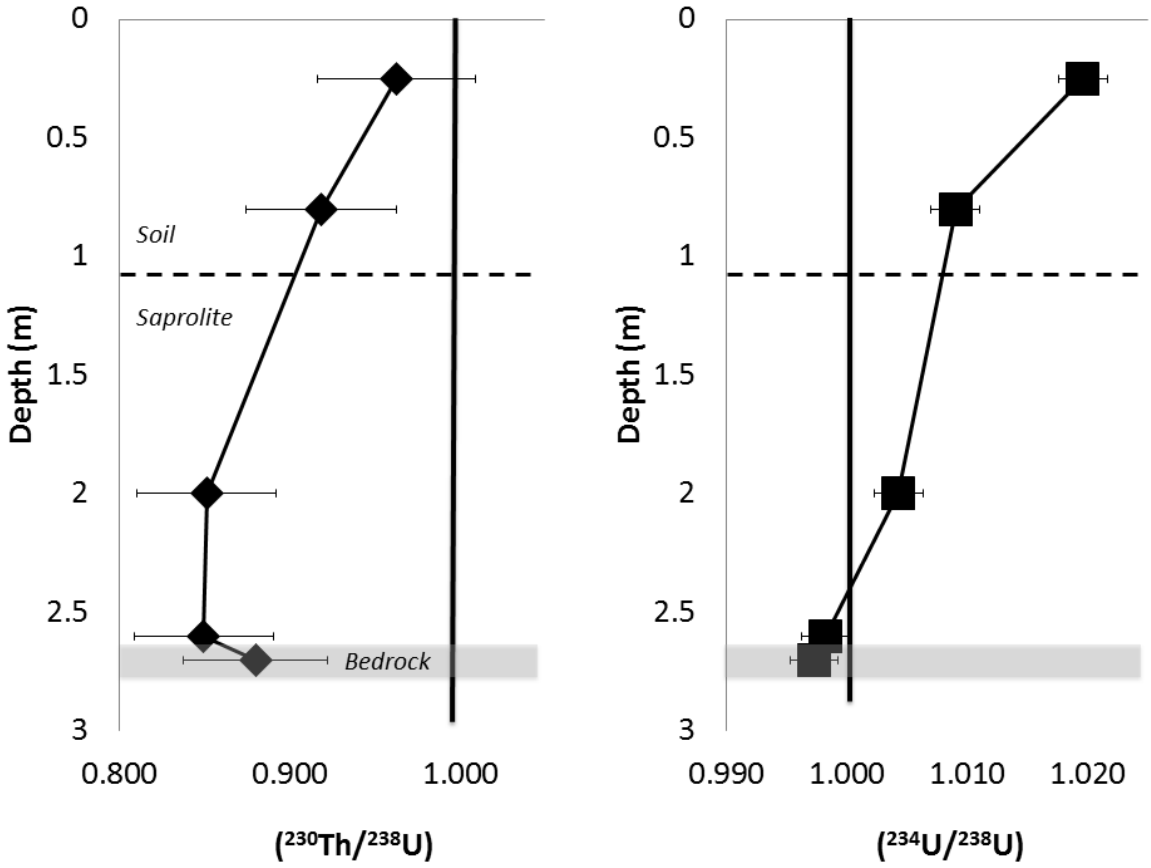

808

809 **Figure 6. ($^{234}U/^{238}U$) and ($^{230}Th/^{238}U$) activity ratios for untreated samples. The dashed line represents the boundary**
810 **between soil and saprolite, while the solid line represents secular equilibrium. Error bars represent external relative**
811 **analytical uncertainties (RSE) reported in Tab. 3.**

812

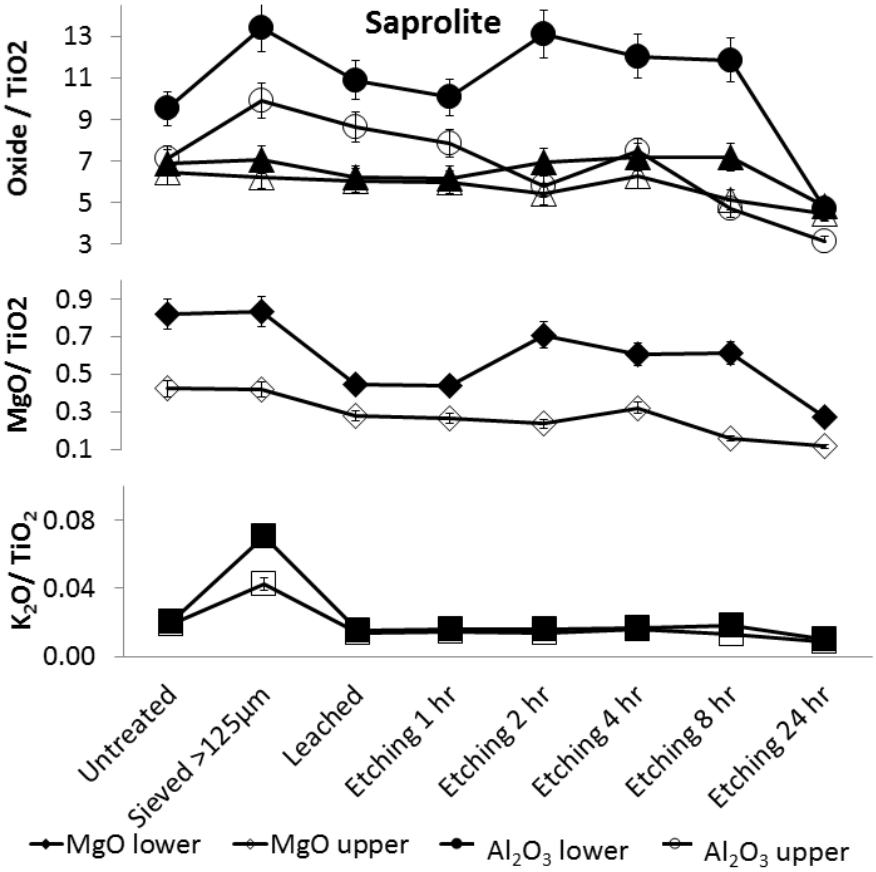

Figure 7. Magnesium, K, Fe and Al oxides to TiO_2 ratios for untreated, sieved, leached and etched saprolite. Close symbols represent the lower saprolite, while the open symbols the upper saprolite. Error bars represent propagated external relative analytical uncertainties (RSE) reported in Tab. 2.

820

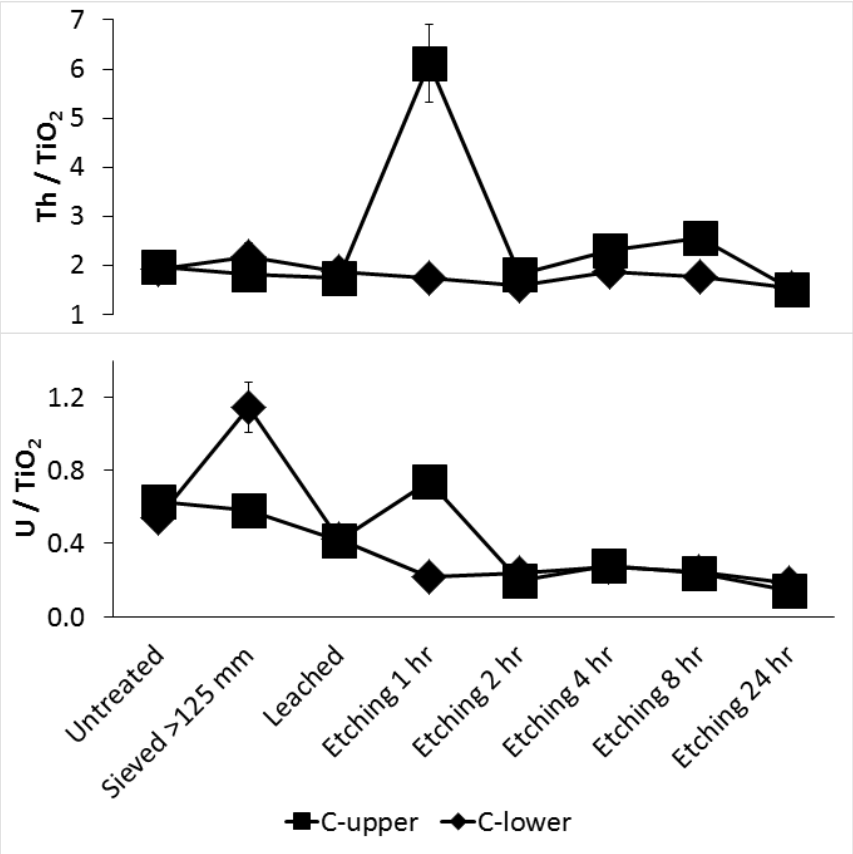

821

822 **Figure 8. U and Th to TiO_2 ratios for the untreated, leached and etched upper and lower saprolite. Error bars**
823 **represent propagated external relative analytical uncertainties (RSE) reported in Tab. 3.**

824

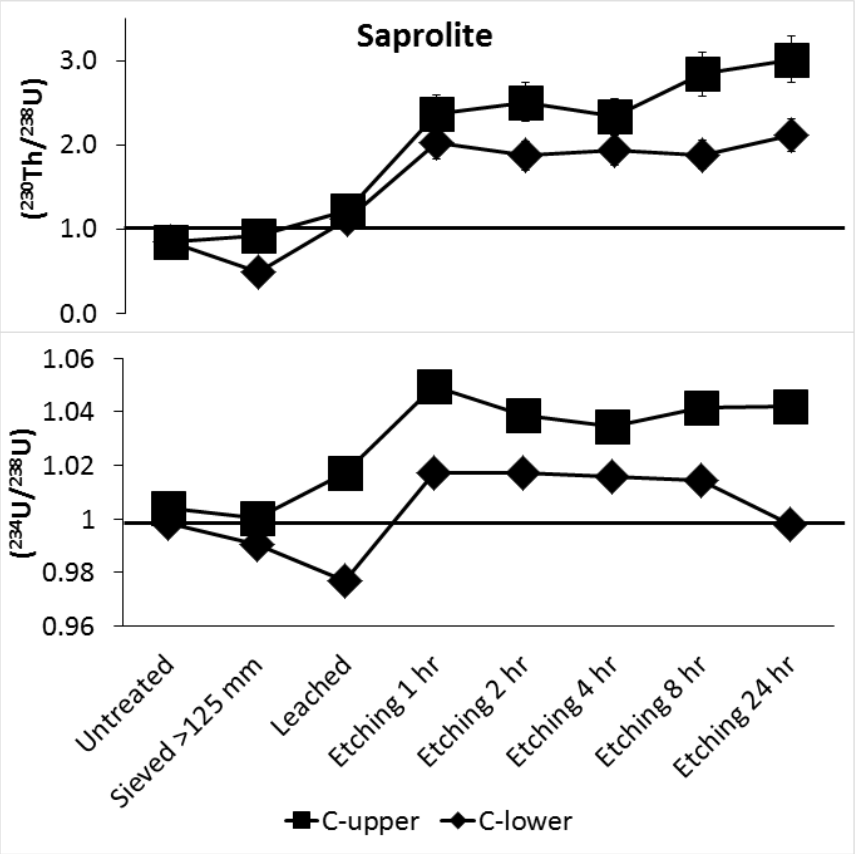

825

826 **Figure 9. ($^{230}Th/^{238}U$) and ($^{234}U/^{238}U$) for the untreated, leached and etched upper and lower saprolite. Error bars**
827 **represent propagated external relative analytical uncertainties (RSE) reported in Tab. 3.**

828

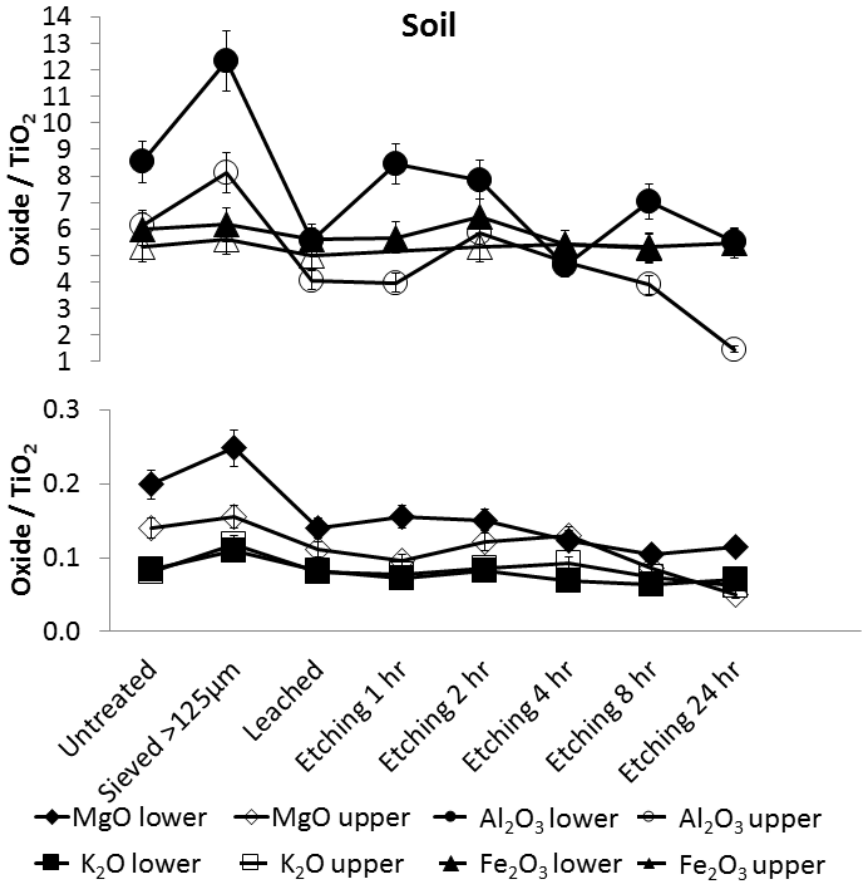

829

830 **Figure 10. Mg, K, Fe and Al oxides to TiO_2 ratios for untreated, sieved, leached and etched soil. Close symbols represent**
831 **the lower soil, while the open symbols the upper soil. Error bars represent propagated external relative analytical**
832 **uncertainties (RSE) reported in Tab. 2.**

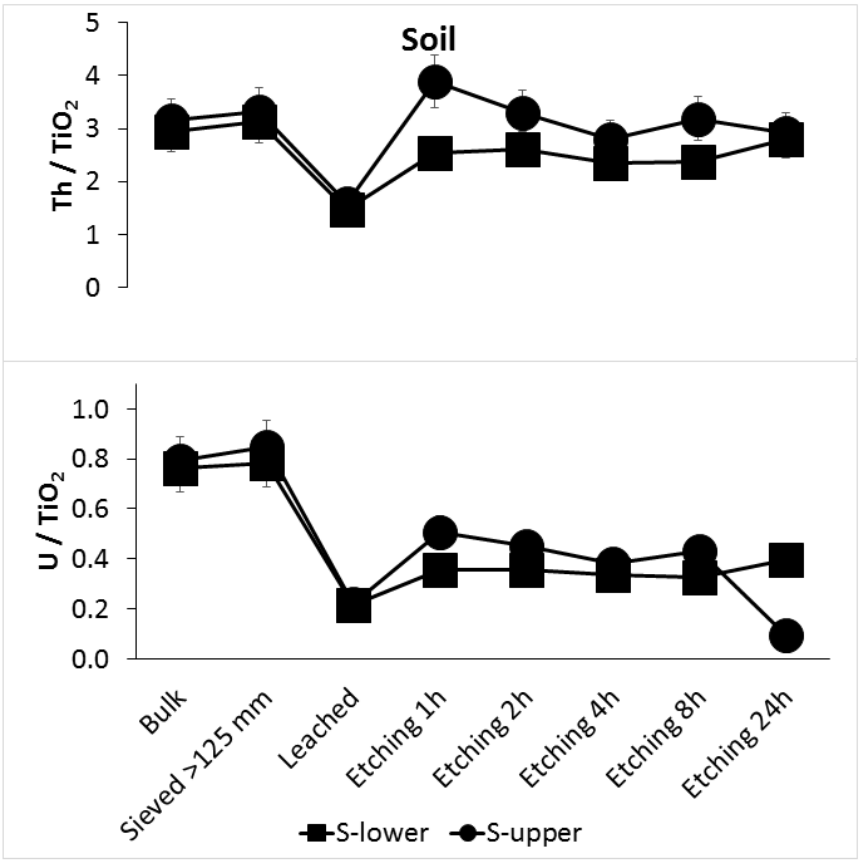

833

834 **Figure 11. U and Th to TiO_2 ratios for the untreated, leached and etched upper and lower soil. Error bars represent**
835 **propagated external relative analytical uncertainties (RSE) reported in Tab. 3.**

836

837

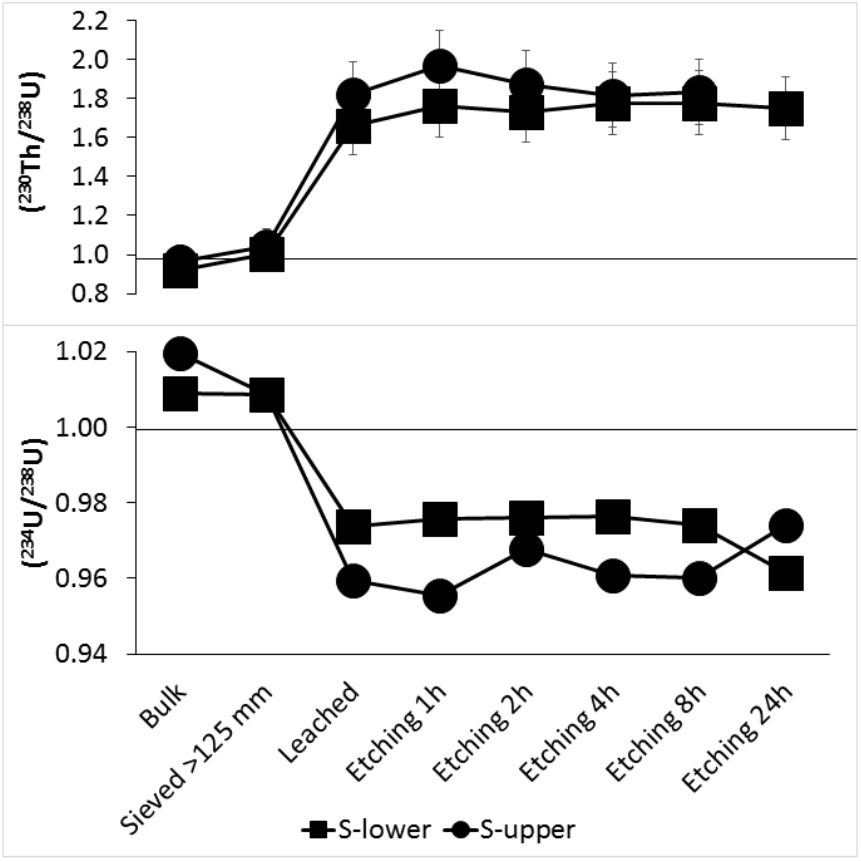

838

839 **Figure 12. (^{230}Th/^{238}U) and (^{234}U/^{238}U) for the untreated, leached and etched upper and lower soil. Error bars**
840 **represent propagated external relative analytical uncertainties (RSE) reported in Tab. 3.**

841

842